COUNTER TUBE WINDOW AND
X-RAY FLUORESCENCE ANALYZER STUDY

By

Dr. R. Hertel and M. Holm

Revised
March 20, 1973
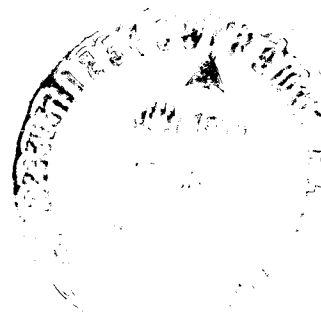
COUNTER TUBE WINDOW AND X-RAY FLUORESCENCE ANALYZER STUDY

BY

DR. R. HERTEL and M. HOLM

Revised
March 20, 1973

UMC 1116-FR

TABLE OF CONTENTS

CONTENTS (Cont'd)

LIST OF ILLUSTRATIONS

ILLUSTRATIONS (Cont'd)

LIST OF TABLES

1.0   INTRODUCTION

This report summarizes a study performed to determine the best design of a counter tube window and X-RAY FLUORESCENCE ANALYZER for quantitative analysis of Venusian dust and condensates. The project was conducted by Universal Monitor Corporation for the Ames Research Center under Contract No. NAS2-7356.

1.1   OBJECTIVES

The principal objective of the project was to develop the best counter tube window geometry for the sensing element of the instrument. This included formulation of a mathematical model of the window and optimization of its parameters.

Other objectives of the project were to:

1. Determine preliminary instrument specifications.

2. Define the overall configuration and components required for a flight instrument.

3. Determine instrument-spacecraft interface requirements.

1.2   KEY FEATURES

The proposed detector and instrument (see Figure 1) has several important features. For example, the instrument will perform a near real-time analysis of dust in the Venusian atmosphere. The instrument is capable of measuring dust layers less than 1 micron thick. In addition, because sample characteristics are presently unknown, a wide dynamic measurement range will be provided to compensate for extreme variations in count rates.

An integral pulse-height analyzer and memory accumulate data and read out spectra for detail computer analysis on the ground.

1

PRESSURE
HOUSING

HEMI-
SPHERICAL
SAMPLE WINDOW

FLUORESCENT
X-RAYS

PRIMARY
X-RAY SOURCE

DETECTOR
WALL

PRIMARY
X-RAYS

1 MIL DETECTOR
WINDOW

HIGH ENERGY
DETECTOR B

LOW ENERGY
DETECTOR A

THERMAL ISOLATION
AND DETECTOR SUPPORT

PRESSURE
SHELL

EXPERIMENT
ELECTRONICS
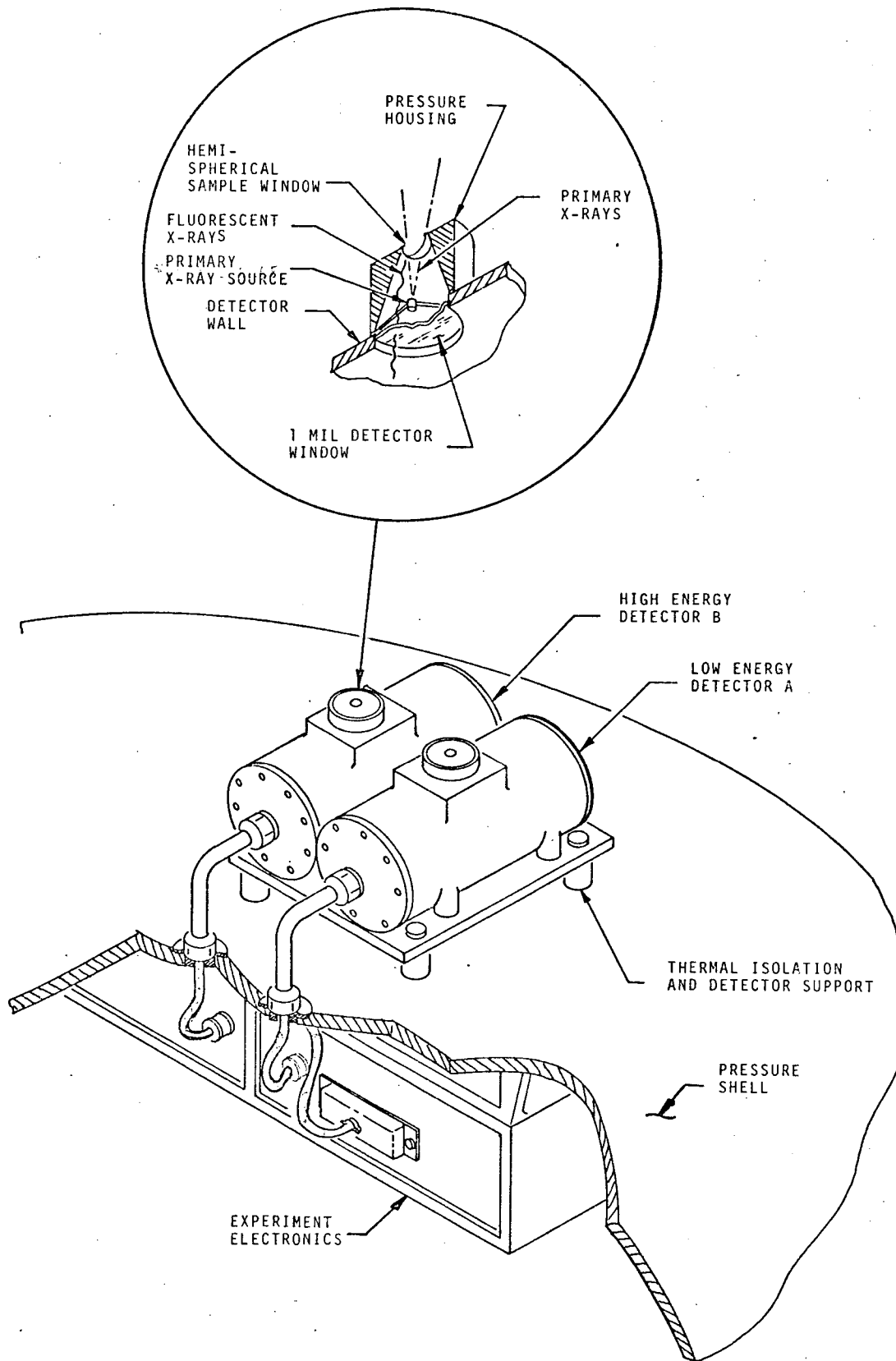
Figure 1. X-Ray Fluorescence Instrument

COST BREAKDOWN

PHASE III - FABRICATE PROTOTYPE

LABOR

Category	Hours	Rate	Total
Physicist	100	$10.00	$ 1,000
Project Manager	300	14.00	4,200
Mechanical Engineer	210	9.00	1,890
Electronic Engineer	360	8.00	2,880
Sr. Electronic Technician	740	6.00	4,440
Draftsman	190	4.50	855
Assembler	1800	4.50	8,100

	$ 23,365
Overhead (112%)	26,169
	$ 49,534
MATERIAL (Instrument and GSE)	30,000
SUBCONTRACTS (includes radiation sources)	38,000
TRAVEL: Ames (2 men x 2 days x 5 trips)*	590
East Coast (2 men x 2 days x 2 trips)**	1,760
CONSULTANT	-0-
ODC (Environmental testing)	1,000
	$120,884
G&A (15%)	18,133
	$139,017
Fee (12%)	16,682
TOTAL PRICE	$155,699

---

*[$34 x 2 x 5] + [$50 x 5] = 340 + 250 = $590

**[$340 x 2 x 2] + [$50 x 2 x 2 x 2] = 1360 + 400 = $1,760

2 -a

Standard, proven and space-instrument flown electronic design techniques are additional key features of the proposed instrument. The experimental technique has already been successfully developed and used on past flight instruments and is presently used in laboratory analysis of complex materials. However, detailed mechanical and electrical design of the instrument still remains to be completed.

Physical characteristics of the instrument which are of major importance because of their interaction with the spacecraft include light weight, low power consumption, and small size. Estimated values are as follows:

Weight: 4.9 lb (2.22 kg)

Volume: 168 in^3 (2.75 x 10^{-3} m^3)

Power Consumption: 2W

A summary set of specifications for the instrument is given in Section 4.1.

1.3   CONCLUSIONS

Feasibility of an X-RAY FLUORESCENCE ANALYZER for study of Venusian dust and condensates has been demonstrated analytically, based on actual hardware used on past programs or now used in the laboratory. Detailed development can be completed within the program schedule of the Venusian Pioneer spacecraft mission. However, an earlier start on the development of the detector window is important to assure thorough design, analysis, and evaluation of this critical component. It is strongly recommended that work begin immediately to assure maximum reliability.

The use of the X-RAY ANALYZER will support present mission objectives and does not impose special or unusual constraints or requirements on the spacecraft or the data system.

1.4   PLAN OF REPORT

The following sections describe background and problems that lead up to the need for the analysis of dust in the Venusian atmosphere; a detailed description of the window, source, detector, and electronics; and a summary of the project results. Circuit analyses, power calculations, and parts lists are included in the appendixes.

2.0 BACKGROUND AND STATEMENT OF PROBLEM

Despite the fact that Venus is Earth's nearest neighbor, remarkably little is known about this planet. Earth-based astronomers have determined the orbital parameters, diameter, density and albedo of Venus, and some spectroscopic determinations were made on the chemical constitution of its atmosphere. No surface markings have ever been observed, and the high albedo implied a heavy cloud layer.

Detailed information has come from U. S. and Russian space probes -- both fly-by and lander. The most recent have been the Russian Venus 7 and Venus 8 missions which have shown the atmosphere to be 97 percent carbon dioxide, about 2 percent nitrogen and possibly 1 percent water vapor, with surface pressures of 90 $\pm$1.5 atmospheres (90 x 10^5 N/m^2). Both day and night surface temperatures were about 470°C (743°K). The surface layer of soil was very loose with a density of about 1.5 times that of water. A gamma-ray spectrometer detected the presence of potassium (4 percent), uranium (0.002 percent) and thorium (0.00065 percent).

The 1976/1977 Pioneer Venus probe mission offers an opportunity to supplement these data with an intensive program of measurements designed to provide information regarding the dynamical and chemical nature of the clouds and atmosphere surrounding Venus with instrumented probes parachuted to the surface. This mission also offers an opportunity to learn something about the chemical composition of the Venusian surface by analyzing dust particles suspended in the atmosphere. An X-RAY FLUORESCENCE ANALYZER can perform 10 to 12 analyses on dust particles collected during the 2-hour descent to the surface, processing the raw data in situ with results of the analyses presented to telemetry.   .

The dynamic range should be great enough to permit metallic elements in the range between sodium and zinc to be detected in dust layers 1 micron (1 x 10^{-6} m) thick as well as in layers of essentially infinite thickness. The instrument must be able to survive the rigors of the launch environment, the cold and vacuum of deep space, and then be able to operate in the extremes of the Venusian

4

environment with high reliability. No failure mode of the X-RAY FLUORESCENCE ANALYZER will compromise or endanger the operation of any other experiments on the probe, or the functioning of the probe itself.

The following sections describe an instrument system which meets these requirements.

3.0 WINDOW DESIGN

This section presents the theoretical design aspects of the counter tube window and a recommended window configuration.

3.1 THEORETICAL STUDY

The following theoretical discussion covers window stress analysis, development of a mathematical model, and design calculations.

3.1.1 Stress Analysis

Two windows are required for the Venusian X-RAY FLUORESCENCE ANALYZER to interface between the three environments involved. The first of these environments is the Venusian atmosphere which at the surface has a pressure of 90 atmospheres (9.1×10^6 N/m^2) and a temperature of 470°C (743°K). The second is an evacuated region containing the primary radiation source. And the third is the proportional counter chamber containing an inert gas at a pressure of approximately 1 atmosphere (1×10^5 N/m^2) and at a temperature somewhat lower than that of the external atmosphere. In addition to withstanding these environmental stresses the windows must be relatively transparent to the fluorescent x-rays, some of which have energies barely above 1 keV. Beryllium is the only material currently available from which windows meeting the above qualifications can be fabricated. The following analyses relate exclusively to this material.

Little reliable information concerning the engineering properties of beryllium in ingot form is available. and even less is known about the properties of foil for which no dependable data on yield strength, tensile strength and Poisson ratio have been published. The values used in this analysis are in part based upon personal experience and in part upon that of the major suppliers and fabricators of beryllium. Working stresses of 25,000 psi (1.72×10^8 N/m^2) for thin beryllium foil

and 21,000 psi (1.45×10^8 N/m^2) for bar stock have been adopted and are believed to be conservative at 500°C (773°K).

Four window designs were analyzed to determine a characteristic dimension (e.g., diameter or width) as a function of thickness which would withstand a pressure differential of 100 atmospheres (1.01×10^7 N/m^2) at 500°C (773°K). These are (a) a long hemicylinder, (b) a hemisphere, (c) a flat circular plate, and (d) a flat rectangular plate. Two window designs were analyzed to determine relevant dimensions which would withstand a differential pressure of one atmosphere at 500°C (773°K). These are a flat circular plate with built-in edges, and an identical plate with four supporting ribs located along radii 90° apart.

(a) The entire length of the edges of the hemicylinder are assumed to be supported (Figure 2a), thus eliminating major bending moments. The stress s is given by

$$s = pr/t$$

where p is the applied pressure, r is the radius, and t the wall thickness. If the window is fabricated from foil, a value for s of 25,000 psi (1.72×10^8 N/m^2) is appropriate. Then, with p = 1470 psi (1.01×10^7 N/m^2),

$$r = st/p$$

$$= 17.0t$$

This relationship is plotted in Figure 3.

(b) The hemisphere is similarly assumed to be supported along the edge. The maximum stress is then a combination of the meridional and hoop stresses and is given by

$$s = 2^{\frac{1}{2}}pr/2t$$

Assuming the window to be machined out of bar stock, the value of s would be 21,000 psi (1.45×10^8 N/m^2). Again taking p to be 1470 psi (1.01×10^7 N/m^2).

$$r = 2^{\frac{1}{2}}st/p$$

$$= 20.2t$$
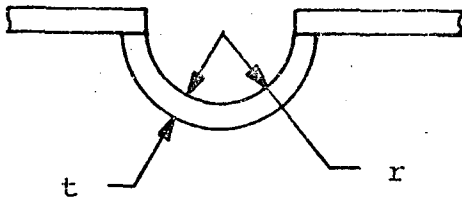
2a
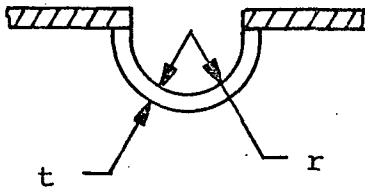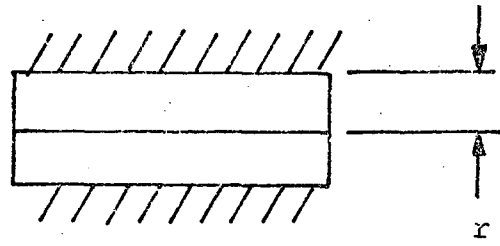
2b
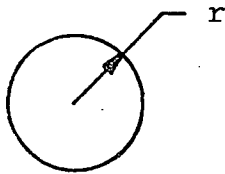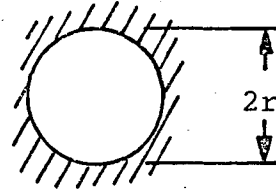
2c
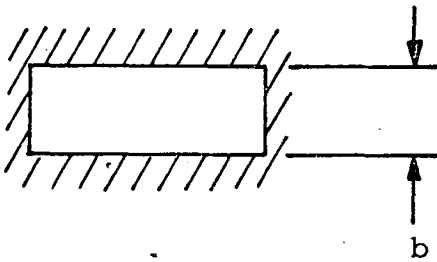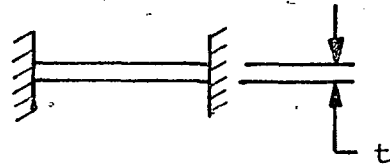
2d
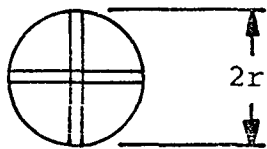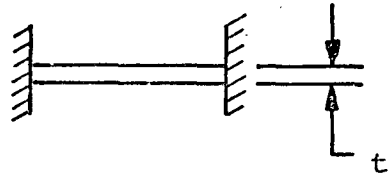
2e
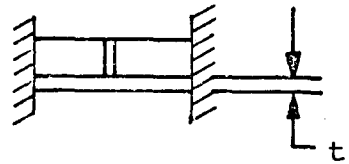
Figure 2.   Window Designs

This relationship is plotted in Figure 3. If, after machining, the beryllium is cold-worked, the higher working stress can be used, giving

$$r = 24.0t$$

Cold-working could result from subjecting the window to a stress sufficient to cause the material to yield slightly and take a set, or it could be peened with glass beads.

(c) The flat circular plate is assumed to have built-in edges (Figure 2c) and to be uniformly loaded over the entire surface. The maximum stress occurs at the edge and is given by

$$s = 3pr^2/4t^2$$

Assuming the window to be made of foil,

$$r = 2(s/3p)^{\frac{1}{2}}t$$

$$= 4.76t$$

This relationship is also plotted in Figure 3.

(d) The flat rectangular plate is assumed to have a large length-to-width ratio and to have built-in edges (Figure 2d). The maximum stress is at the center of a long edge and is given by

$$s = pb^2/2t^2$$

where b is the width of the rectangle. If the window is fabricated from foil, s = 25,000 psi (1.72 x 10^8 N/m^2). With p = 1470 psi (1.01 x 10^7 N/m^2),

$$b = (2s/p)^{\frac{1}{2}}t$$

$$= 5.83t$$

A plot of this expression is shown in Figure 3.

For the unsupported low pressure window, the analysis in (c) can be used by substituting 14.7 psi (1.01 x 10^5 N/m^2) for p instead of 1470. Since r is inversely proportional to the square root of the pressure, decreasing the pressure by a factor of 100 increases the radius by a factor of 10, giving

$$r = 47.6t$$
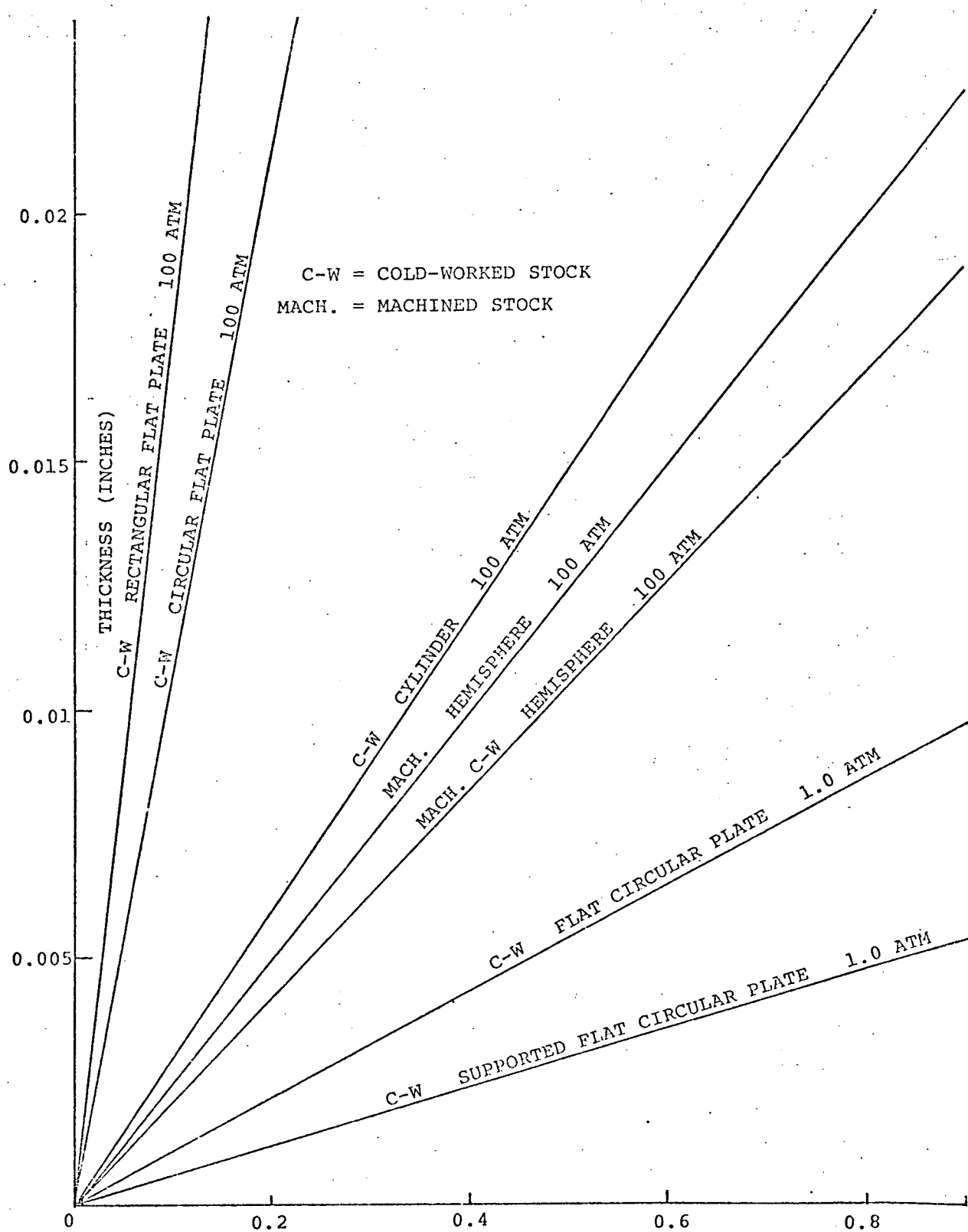
Figure 3. Characteristic Dimension (Inches)

Figure 2e shows a flat circular plate with built-in edges and four supporting ribs. For this configuration the stress is

$$s = 0.145\ p(r/t)^2$$

Using the working stress for foil and a pressure of 14.7 psi (1.01×10^5 N/m^2),

$$r = (6.9\underline{0}^*s/p)^{\frac{1}{2}}t$$

$$= 108.3t$$

These relationships for the low-pressure window have also been plotted in Figure 3.

Hemispherical geometry was given preference over the other geometries considered for the high-pressure window for the following reasons:

(a) For a given thickness of beryllium, the useful area is greatest in this geometry;

(b) The mechanical reliability is maximized because the total area of window is less for a given useful area and the length of edge which must be welded is shorter than for other geometries;

(c) Fabrication of the collimating shield for the primary x-ray source is at least an order of magnitude less difficult for a given source solid angle with spherical geometry than with cylindrical geometry (the only seriously competitive geometry);

(d) Fabrication of the window itself is significantly less difficult in spherical geometry than in cylindrical geometry.

A flat circular geometry was selected for the low-pressure window because it is easy to fabricate in the required thickness, and because it offers the maximum solid angle as seen from secondary-emitting dust particles on the upper window.

---

* Bar under digit indicates it was rounded up to nearest integer.

3.1.2 Mathematical Model

The window assembly consists of a hemispherical beryllium window of radius r_2 and thickness t_2 mounted on a truncated cone of half-angle δ and length ℓ. A source of strength S curies and fluorescent yield w_1 is positioned on the axis of the support cone a distance y below the window. A lower beryllium window of essentially plane configuration and thickness t_3 provides access to the proportional counter. The source is collimated to produce a cone of primary x-rays of half-angle α_o which will not be able to reach the lower window without undergoing multiple scattering. A schematic representation is shown in Figure 4.

Scattering of x-rays is proportional to the atomic number of the scattering medium and is greater for soft than for hard x-rays. Collimating the source so that primary rays can not reach the support cone reduces the useful area of the window to some extent, but this simplifies the window fabrication problem by minimizing the area where the beryllium must be very thin, and it performs the more important function of minimizing scat-tered primary radiation. Such radiation contributes to the background count rate and could obscure counts of fluorescent x-rays because of counter dead time. Compton scattering could alternatively give rise to false positives. If the support cone were made from a very low-Z material such as beryllium , the beam of primary rays could be opened up to include a greater area of the upper window without resulting in a serious increase in the scattered primary radiation. The resulting increase in count rate would be small, however, since primary and secondary rays in this added area penetrate window and dust at large angles of inci-

Revised 3/20/73
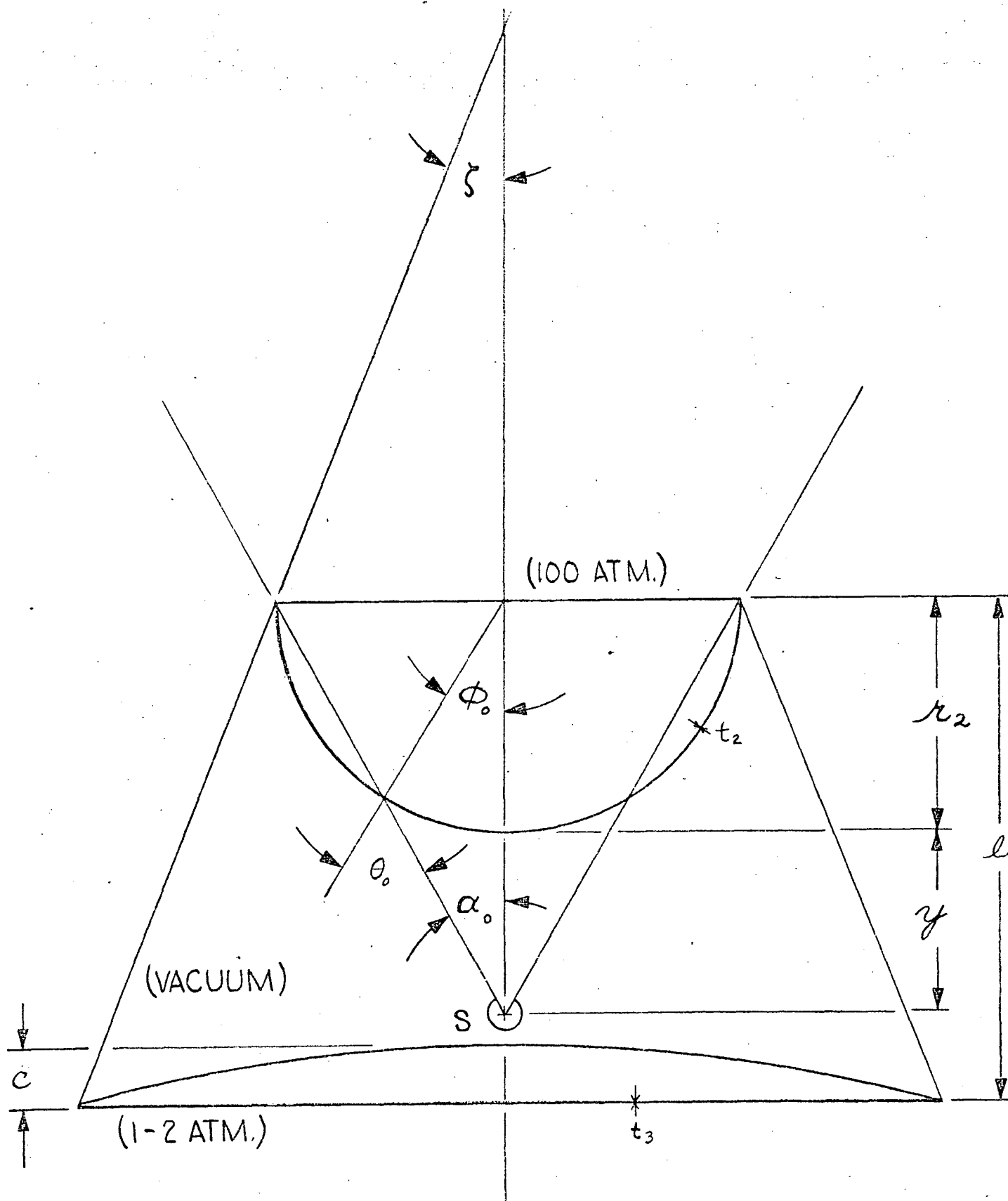
Figure 4. Hemispherical Window --
Point Source Configuration

13

dence and suffer greater losses from absorption. The increased costs of beryllium fabrication techniques would not justify the resultant increase in count rate. For these reasons, a support cone of higher Z material such as stainless steel, relatively easy to machine and weld, is proposed along with source collimation designed to minimize scattered primary rays.

The cone of primary rays subtends a solid angle Γ_0 which for a point source is given by

$$\Gamma_0 (r_2, y) = 2\pi(1 - \cos\alpha_0)$$
$$= 2\pi[1 - (r_2+y)/(2r_2^2+2r_2y+y^2)^{1/2}]$$

since $\alpha_0 = \tan^{-1}[r_2/(r_2+y)]$. The useful area of the window (that part irradiated by primary radiation) is given by

$$U(r_2, y) = 2\pi r_2^2(1 - \cos\phi_0)$$
$$= 2\pi r_2^2(1 - 2\sin\alpha_0\cos\alpha_0)$$
$$= 2\pi r_2^2 \, y^2/(2r_2^2+2r_2y+y^2)$$

since $\phi_0 = \pi/2 - 2\alpha_0$ (see Fig. 4). The angle of incidence of the extreme primary rays as they enter the window is

$$\theta_0 = \pi/2 - \alpha_0.$$

In the general case, a ray making an angle α with the central axis will enter the window at an angle of incidence θ_1 given by

$$\theta_1 = \sin^{-1}[(r_2+y)\sin\alpha/r_2]$$

14   Revised 3/20/73

Consider an annular area $A(\alpha, d\alpha)$ on the upper window and the conical shell of primary radiation passing through A of solid angle $d\Gamma$ given by (Fig. 6)

$$d\Gamma = 2\pi \sin \alpha \, d\alpha$$

In the following discussion, $A(\alpha, d\alpha)$ will refer not only to the region on the upper window defined by $d\Gamma$ but also to the adjacent annular region in the dust on the window defined by $d\Gamma$. The number of primary photons incident on the lower surface of the window contained in $d\Gamma$ is

$$dN_o (\alpha, d\alpha) = P_p (d\Gamma / 4\pi) A_s \qquad s^{-1}$$

where P_p is the primary Production term equal to 3.7×10^{10} S w_1 photons per second, A_s is the source Absorption term equal to $[1 - \exp(-\mu_1 t_1)]/\mu_1 t_1$, μ_1 is the linear absorption coefficient for primary x-rays in the source material (Fe/Mn or Cd/Ag), and t_1 is the thickness of source material. The number emerging on the other side and entering any Venusian dust trapped on the window is

$$dN_e (\alpha, d\alpha) = dN_o A_{B1p} \qquad s^{-1}$$

where A_{B1p} is the Absorption term for primary rays in Beryllium window number 1 (upper window) and equal to $\exp(-\mu_2 t_2 \sec \theta_1)$, and μ_2 is the linear absorption coefficient for primary radiation in beryllium.

The number of primary rays absorbed by a dust layer of thickness dh at a depth h from the window surface by atoms of species i is then given by

15

$$dN_i(\alpha, d\alpha, h, dh) = dN_e \, A_{Dp} \, \mu_{ip} \sec \theta_l \, dh \qquad s^{-1}$$

where A_{Dp} is the <u>A</u>bsorption term for <u>p</u>rimary radiation in <u>D</u>ust equal to $\exp(-\mu_3 h \sec \theta_l)$, μ_3 is the linear absorption coefficient for primary rays in the dust composite, and μ_{ip} is the linear absorption coefficient for <u>p</u>rimary radiation by atoms of species <u>i</u> in the dust particles. Finally, the number of <u>s</u>econdary rays emitted (<u>P</u>roduced) by atoms of species <u>i</u> in the dust in dh at h from excitation by primary rays in $d\Gamma$ is

$$dP_{si}(\alpha, d\alpha, h, dh) = dN_i \, w_i \qquad s^{-1}$$

where w_i is the fluorescent yield of atoms of species i in the dust. This is an approximate expression since it ignores primary radiation scattered into $A(\alpha, d\alpha)$ from neighboring portions of the window and dust outside of $d\Gamma$. The actual value is slightly larger, but the error is small since the window is a very low Z material, the dust is moderately low Z and low density, and the scattering is predominantly forward.

Referring to Figures 5 and 6, Ω is the solid angle subtended by the lower window from dA, an element of $A(\alpha, d\alpha)$. Γ_o, the solid angle subtended by the rim of the upper window, contains all of the useable primary photons. Ω contains all of the secondary (fluorescent) rays from dA which can reach the counter through the lower window. Let $d\Omega$ be an element of Ω whose projection on the lower window is dK = dx dz. $d\Omega$ makes an angle θ_2 with $\overline{OR}$, the normal to the window surface at dA, and it makes an angle ψ with the normal to the surface of the lower window at dK. Because of symmetry, the entire contribution from fluorescent sources in the

Revised 3/20/73
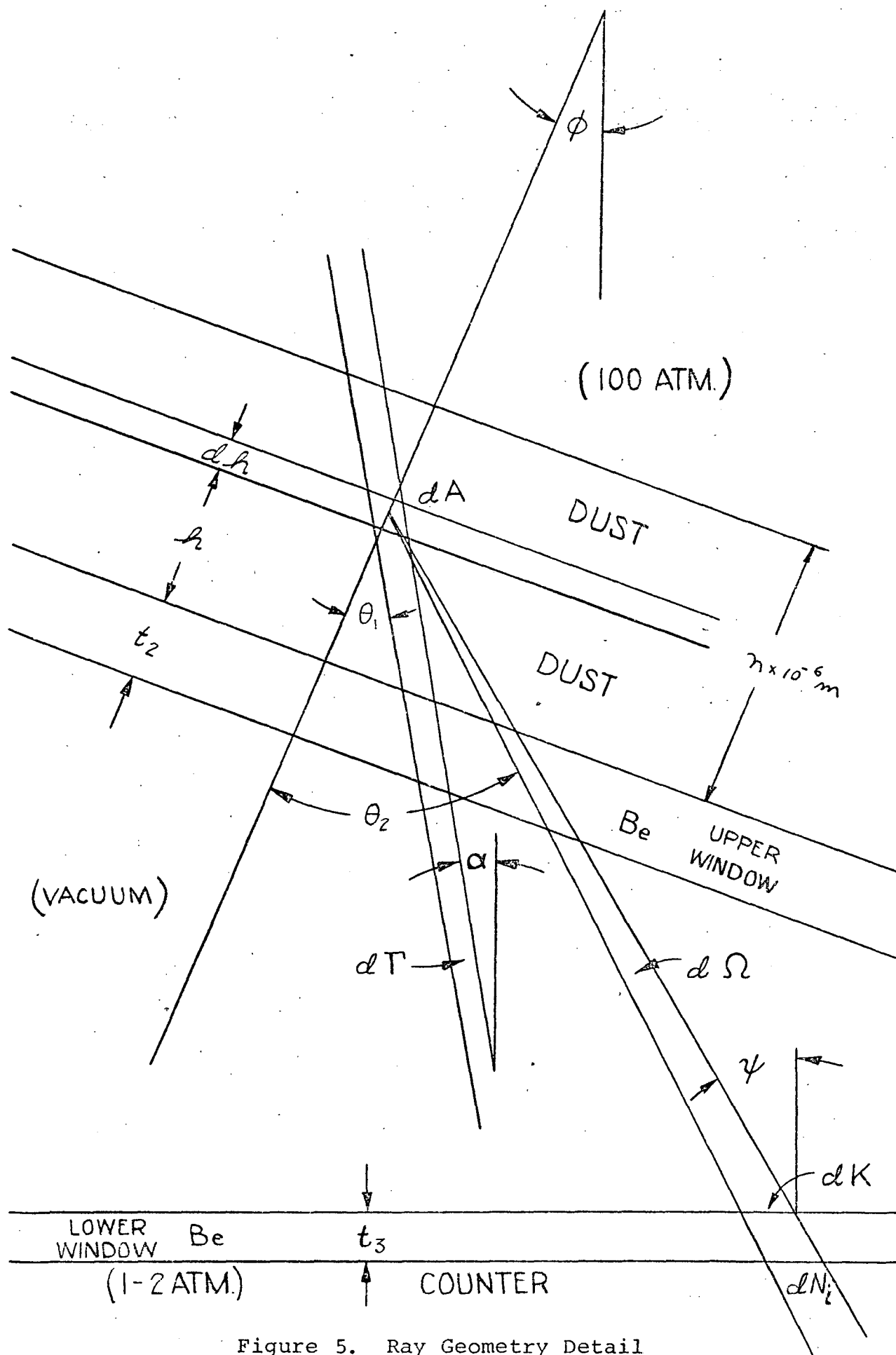
Figure 5. Ray Geometry Detail

Figure 6. Secondary Ray Geometry
in Three Dimensions

region $A(\alpha, d\alpha)$ of the dust excited by primaries in $d\Gamma$ can be considered to be coming from dA. Consequently, it is unnecessary to perform an integration over the azimuthal angle.

The number of secondary or fluorescent photons in $d\Omega$ which originate in atoms of species i in a dust layer of thickness dh a distance h above the upper window and which ultimately enter the active volume of the counter can be written as

$$dC_i(\alpha, d\alpha, h, dh) = dP_{si}(d\Omega/4\pi) \; A_{Dsi} \; A_{B1si} \; A_{B2si}$$

where A_{Dsi} is the Absorption in Dust of secondary rays from atoms of species i, equal to $\exp(-\mu_{ij} h \sec \theta_2)$; A_{B1si} is the Absorption in Beryllium window number 1 (upper window) of secondary photons from atoms of species i, equal to $\exp(-\mu_{ik}t_2 \sec \theta_2)$; A_{B2si} is the Absorption in Beryllium window number 2 (lower window) of secondary photons from atoms of species i, equal to $\exp(-\mu_{ik}t_3 \sec \psi)$; μ_{ij} is the linear absorption coefficient for fluorescent ($K\alpha$) x-rays from atoms of species i in the dust composite; and μ_{ik} is the linear absorption coefficient for secondary ($K\alpha$) rays from atoms of species i in beryllium. $d\Omega$ is the element of solid angle subtended by dK from dA, given by

$$d\Omega = dx \, dz \cos \psi / [a^2 + x^2 + (d+z)^2]$$

where $a = \ell - r_2 \cos \phi$, $d = [y + r_2(1 - \cos \phi)] \tan \alpha$, $\phi = \theta_1 - \alpha$, and $\cos \psi = a/[a^2 + x^2 + (d+z)^2]^{1/2}$.

The angle θ_2 is at the apex of a triangle whose sides are line segments joining dA with the point R and with dK, and whose base is a line segment joining R and dK. Call these line segments respectively e, f, and g. Then,

19

Revised 3/20/73

$$\cos \theta_2 = (e^2 + f^2 - g^2)/2ef$$

where

$$e = a \sec \phi$$

$$f = [a^2 + x^2 + (d+z)^2]^{1/2}$$

$$g = [x^2 + (d+z)^2]^{1/2}$$

Thus,

$$\sec \theta_2 = 2ef/(a^2 + e^2)$$
$$= 2ef/a^2(1 + \sec^2\phi)$$

C_i, the number of $\underline{C}$ounts per second recorded by the proportional counter of fluorescent x-ray photons from atoms of species $\underline{i}$ in the dust, is found by integrating the expression for dC_i. The limits for the integrals are as follows:

$d\Gamma$: $\alpha = 0$ to $\alpha = \alpha_0$

dP_{si}: $h = 0$ to $h = n \times 10^{-4}$ cm   ($1 \leqq n \leqq 100$)

$d\Omega$: $x = -r_3$ to $x = +r_3$

$z = -(r_3{}^2 - x^2)^{1/2}$ to $+(r_3{}^2 - x^2)^{1/2}$

where $r_3 = r_2 + \ell \tan \zeta$.

The linear absorption coefficients for primary photons and fluorescent Kα rays in dust, μ_3 and μ_{ij} respectively, are summations of the form

$$\mu_3 = \sum_i \delta_i \mu_{pi}$$

$$\mu_{ij} = \sum_h \delta_h \mu_{ih}$$

where the δ's are weighting factors depending upon the assumed composition of the dust.

3.1.3 Window Design Calculations

Values of C_i were calculated for Fe^{55} and Cd^{109} x-ray sources with olivine and silica dust on the window. A standard source strength of 100 millicuries was adopted and the parameters chosen for systematic variation were (i) y, the source-window distance, (ii) ζ, the support-cone half-angle, and (iii) n, specifying the thickness of the dust layer.

Fe^{55} atoms decay by electron capture to Mn^{55} atoms in a metastable excited state. The half-life for this transformation is 2.94 years, or 9.27×10^7 seconds. The excited Mn^{55} atoms can return to the ground state in a radiationless transition with the emission of an electron, or with the emission of characteristic Mn x-rays, the most prominent of which are the $K\alpha$ lines with energies of 5.888 and 5.899 keV. Similarly, Cd^{109} decays to Ag^{109} with the ultimate emission of characteristic Ag x-rays having energies of 21.99 and 22.16 keV for the $K\alpha$ lines. The half-life for the Cd^{109}-Ag^{109} transformation is 450 days or 3.89×10^7 seconds. The probability that a metastable atom returns to the ground state with a radiative transition (in this context) is called the fluorescence yield and is denoted by the symbol w_1. In the case of atoms in dust particles excited by interactions

with primary x-ray photons, the probability that the vacancies in the K shells are filled through radiative transitions is denoted by the symbol w_i, where i refers to the species of atom emitting the fluorescent x-rays.

The transformation constant λ is equal to ln $2/T_{1/2}$, where $T_{1/2}$ is the half life expressed in the same units as λ. For the two isotopes in question,

$$\lambda(Fe) = 7.48 \times 10^{-9} \text{ s}^{-1}$$
$$\lambda(Cd) = 1.78 \times 10^{-8} \text{ s}^{-1}$$

In this report the source activity is defined in terms of the number of Fe^{55}-Mn^{55} or Cd^{109}-Ag^{109} transformations occurring in unit time. In a one-Curie source, 3.7×10^{10} transformations are taking place each second by definition. A source of strength S Curies will have N(i) atoms present where

$$N(i) = 3.7 \times 10^{10} \text{ S}/\lambda(i)$$

Thus,

$$N(Fe) = 4.95 \times 10^{18} \text{ S}$$

$$N(Cd) = 2.08 \times 10^{18} \text{ S}$$

In selecting a value for S, consideration must be given to the time which will elapse after the fabrication of the source until the descent into the Venusian atmosphere, for the half lives of both source materials are comparable to this "dormant" period.

The volume of pure source material occupied by the N atoms for S = 0.1 is given by

$$V(i) = N(i) \, M(i)/6.02 \times 10^{23} \, D(i)$$

where M is the molecular weight and D the density of material i. Substituting the appropriate values for iron and cadmium,

$$V(Fe) = 5.75 \times 10^{-6} \text{ cm}^3 \quad (5.75 \times 10^{-12} \text{ m}^3)$$

$$V(Cd) = 4.36 \times 10^{-6} \text{ cm}^3 \quad (4.36 \times 10^{-12} \text{ m}^3)$$

Assuming, for example, a cylindrical source of radius r_1 and thickness $t_1 = 2r_1$,

$$r_1(Fe) = 0.97 \times 10^{-2} \text{ cm} \quad (9.7 \times 10^{-5} \text{ m})$$

$$r_1(Cd) = 0.89 \times 10^{-2} \text{ cm} \quad (8.9 \times 10^{-5} \text{ m})$$

A satisfactory approximation to the source self-shielding term, A_s, can be derived by assuming the emergent primary photons to be collimated into a narrow beam. Let dN be the contribution from a layer dx thick a distance x from the front face of the source:

$$dN = N_o e^{-\mu_1 x} \, dx/t_1$$

where $N_O = 3.7 \times 10^{10} \, S \, w_1 \, \Gamma/4\pi$. The total number of primary photons in Γ is thus approximately

$$N = (N_o/\mu_1 t_1) \int_0^{t_1} e^{-\mu_1 x} (\mu_1 dx)$$

$$= (N_o/\mu_1 t_1) \, (1 - e^{-\mu_1 t_1})$$

For example, with $y = r_2$, $\Gamma = 0.66$ sr, and with S = 0.1,

$$N_o(Fe) = 6.11 \times 10^{7} \quad s^{-1}$$

$$N_o(Cd) = 1.63 \times 10^{8} \quad s^{-1}$$

$$N(Fe) = 4.48 \times 10^{6} \quad s^{-1}$$

$$N(Cd) = 6.71 \times 10^{7} \quad s^{-1}$$

In calculating absorption coefficients in dust, two cases were considered: olivine and silica. The olivine was considered to be made up of 75 percent Forsterite and 25 percent Fayalite. Forsterite, Mg_2SiO_4, has a specific gravity of 3.222 and Fayalite, Fe_2SiO_4, has a specific gravity of 4.392. A solid olivine of the assumed composition would thus have a specific gravity of 0.75 x 3.222 + 0.25 x 4.392 = 3.515. If the dust is made up of rounded particles (not necessarily spherules) of assorted sizes, voids between the particles will account for about 30 percent of the volume. Thus, the density of olivine dust was taken to be 2.46 g/cm^3 (2460 kg/m^3).* The molecular weight is 1.5 x 24.3 + 0.5 x 55.8 + 28.1 + 4 x 16 = 156.5. The partial densities are

Mg: 1.5 x 24.3 x 2.46/156.5 = 0.573 g/cm^3 (573 kg/m^3)

Fe: 0.5 x 55.8 x 2.46/156.5 = 0.439 g/cm^3 (439 kg/m^3)

Si: 1.0 x 28.1 x 2.46/156.5 = 0.442 g/cm^3 (442 kg/m^3)

O: 4.0 x 16.0 x 2.46/156.5 = 1.006 g/cm^3 (1006 kg/m^3)

The following table gives values for the mass absorption coefficients for $K\alpha$ x-rays from various source atoms in the olivine atoms and in beryllium.

Source $K\alpha$	μ/ρ					
	Mg	Fe	Si	O	Be	Cd
Mn	93.8	89.4	145	30.9	2.9	
Ag	2.1	19.7	3.3	0.8	0.1	15.0
Mg	463.6	6121	802	2433	245.6	
Fe	74.6	71.4	115.5	24.5	2.3	
Si	2825	2502	327.9	965.6	96.2	

Values of the linear absorption coefficient are found by multiplying the above coefficients by the appropriate

---

*The presence of CO_2 at 100 atmospheres in the voids does not alter the results significantly.

Revised 3/20/73

partial densities. In silica dust of density 1.86 g/cm^3 (1860 kg/m^3) the partial densities are: Si — 0.87 g/cm^3 (870 kg/m^3); O_2 — 0.99 g/cm^3 (990 kg/m^3).

Source Kα	Olivine				Silica		
	Mg	Fe	Si	O	Si	O	Be
Mn	53.<u>8</u>	39.2	64.1	31.1	126.<u>2</u>	30.6	5.<u>4</u>
Ag	1.2<u>2</u>	8.<u>7</u>	1.4<u>5</u>	0.<u>8</u>	2.<u>9</u>	0.<u>8</u>	0.2
Mg	265.<u>7</u>	2684	354.5	244<u>8</u>	698	240<u>9</u>	454.<u>4</u>
Fe	42.<u>8</u>	31.3	51.<u>1</u>	24.7	10<u>1</u>	24	4.<u>3</u>
Si	1619	1097	145.<u>0</u>	971.4	285	956	178.0

The caption above the table reads: μ cm^{-1}

The absorption coefficients used in the c_i calculations were derived from the above tables. They are listed below for reference where μ(A-B) is the linear absorption coefficient of element or material B for Kα radiations from atoms of species A.

The density of iron is 7.86 g/cm^3 (7860 kg/m^3) and of cadmium 8.64 g/cm^3 (8640 kg/m^3).

μ_1: μ(Mn-Fe) = 702.7; μ(Ag-Cd) = 129.7

μ_2: μ(Mn-Be) = 5.<u>4</u>; μ(Ag-Be) = 0.2

μ_3: μ(Mn-Olivine) = 188.<u>2</u>; μ(Ag-Olivine) = 12.<u>1</u>

   μ(Mn-Silica) = 156.<u>8</u>; μ(Ag-Silica) = 3.6

μ_{ip}(Olivine): μ(Mn-Mg) = 53.<u>8</u>; μ(Ag-Mg) = 1.2<u>2</u>

     μ(Mn-Fe) = 39.2; μ(Ag-Fe) = 8.<u>7</u>

     μ(Mn-Si) = 64.1; μ(Ag-Si) = 1.4<u>5</u>

  (Silica) μ(Mn-Si) = 126.<u>2</u>; μ(Ag-Si) = 2.<u>9</u>

μ_{ij}:　μ(Mg-Olivine) = 5752;　μ(Fe-Olivine) = 149.8

　　　　μ(Si-Olivine) = 3833;

　　　　μ(Si-Silica)　= 1241

μ_{ik}:　μ(Mg-Be) = 454.4

　　　　μ(Fe-Be) =　4.3

　　　　μ(Si-Be) = 178.0

The value of ℓ was taken to be r_2 + y + 0.318, placing the lower window 1/8-inch (3.18 x 10^{-3} m) below the source. An upper window thickness of 0.0056 cm and a lower of 0.0028 cm were assumed.

The solid angle subtended by the source from a point on the upper window directly above the source is

$$\omega(\eta_1) = 2\pi(1 - \cos\eta_1)$$

where

$$\eta_1 = \tan^{-1}[y/(r_1 + t_s)]$$

with t_s being the thickness of shielding about the source. The solid angle subtended by the lower window from the same point on the upper window is

$$\omega(\eta_2) = 2\pi(1 - \cos\eta_2)$$

where

$$\eta_2 = \tan^{-1}[(r_1 + \ell\tan\zeta)/(y + 0.318)]$$

It is assumed that the solid angle subtended by the source from any other point on that part of the upper window irradiated by primary x-rays is the same as $\omega(\eta_1)$. This assumption can be refined when a detailed design of the source and shield, plus supporting spider, is available, but this correction is not expected to change the tenor of these calculations.

26　　　　　　　　　　　　　　　　　　　Revised 3/20/73

Call the value of C_i corrected for the source shadowing effect C_{ic}. We then have

$$C_{ic} = C_i [1 - \omega(\eta_1)/\omega(\eta_2)] = C_i K$$

In the C_i calculations, $r_1 + t_s$ was taken to be 0.05 cm (5 x 10^{-4} m), and r_2 was set equal to 0.127 cm (1.27 x 10^{-3} m). The value of K as a function of y is plotted in Figure 7 for four values of the support cone half-angle ζ.

The results of the calculations are tabulated in Table I. Certain conclusions can be drawn from these data. For example, as would be expected, increasing the support-cone half-angle increases the count rate. However, starting at 22.5° (Fe source, analyzing for Si in silica dust) with y equal to the radius of the upper window, increasing ζ so as to double the lower window area causes an increase in the count rate of 35 percent. Doubling the area again adds only 16 percent to the count rate, and doubling the area once more produces an increment to the count rate of just 7 percent. Clearly, for the geometry postulated, increasing the support-cone half-angle beyond 45° does not increase the count rate enough to justify the increase in fabrication complexity and expense.

Varying y while holding ζ fixed at 45° produces a maximum in the corrected count rate at approximately y = 0.096 cm (9.6 x 10^{-4} m), but the maximum is fairly broad and a 32 percent increase in y results in a decrease in N_{ic} of less than 10 percent.

A 1-micron (1 x 10^{-6}m) thick layer of olivine dust will produce a count rate of 13 per second when analyzing for silicon with a Cd^{109} source and a count rate of 5100 per second when analyzing for iron. The implication is strong that an x-ray fluorescent experiment with a 100-millicurie Cd^{109} source will give meaningful analyses of Venusian dust even if the upper beryllium window is 5 to 10 mils (1.27 x 10^{-4} to 2.54 x 10^{-4} m) thick. The fabrication of such a window in hemispherical form, with a diameter of 0.2 inch is easily possible using current technology of machining to within 10 or 15 mils (2.54 x 10^{-4} or 3.81 x 10^{-4} m) of the finished thickness and chemically etching away the remainder of the unwanted stock. Uniform thickness is not a requirement so long as the thickness does not go below a minimum value, and the
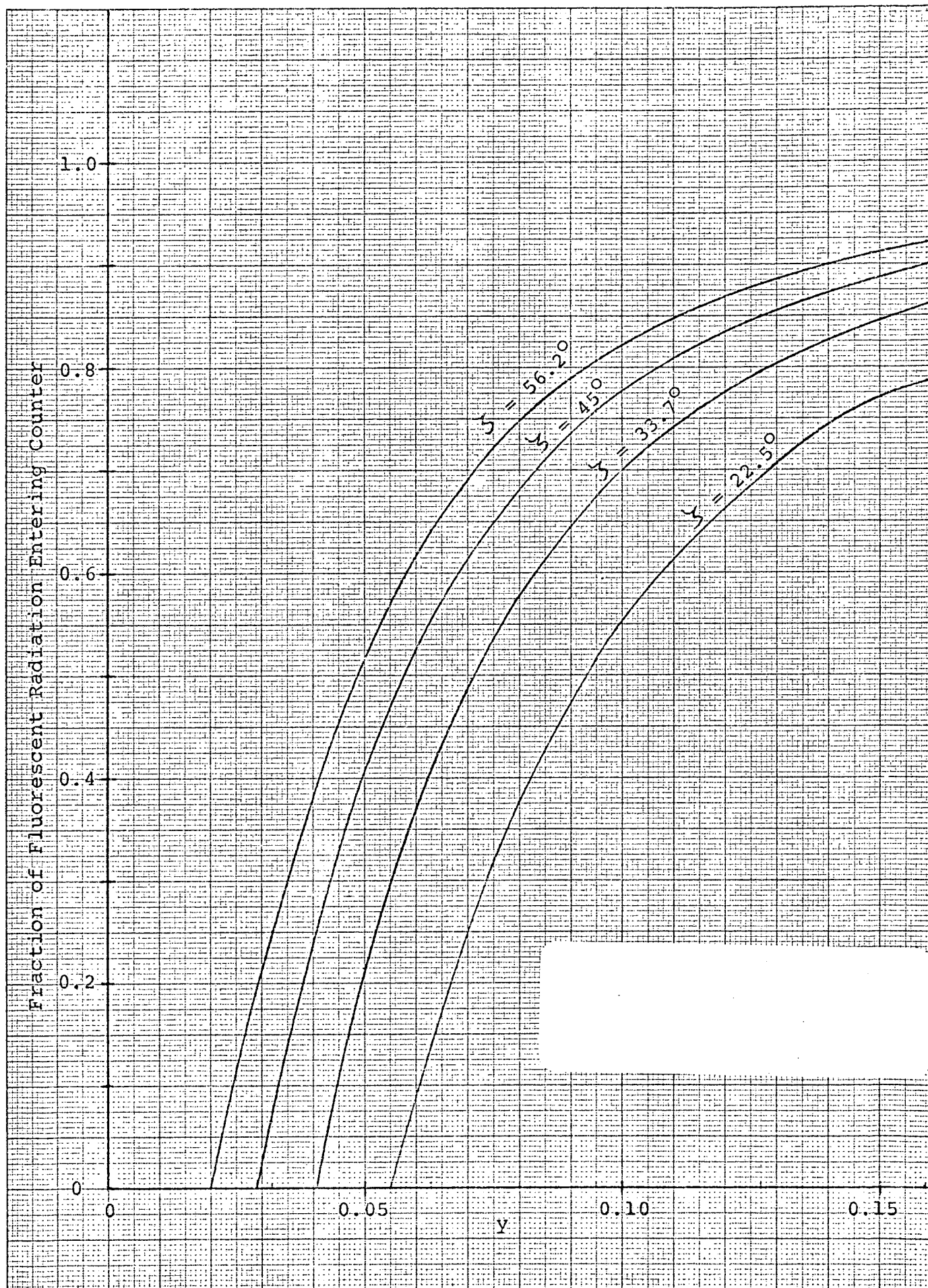
Figure 7.   Shadowing of Counter by Source Assembly

TABLE I. CALCULATED VALUES OF C_{ic}

Source	Dust Material	Element Analyzed	y	ζ	n	C_i (s^{-1})	C_{ic} (s^{-1})
Fe^{55}	Silica	Si	0.032	45°	1	99.9	7.5
			0.063	45°	1	79.2	43.9
			0.095	45°	1	63.6	48.1
			0.127	45°	1	52.0	44.2
			0.159	45°	1	43.2	38.8
			0.127	$22\frac{1}{2}^{O}$	1	33.4	23.2
			0.127	33.8^{O}	1	44.6	35.5
			0.127	$56\frac{1}{4}^{O}$	1	55.8	49.2
			0.032	45°	10	515.4	38.7
			0.063	45°	10	408.8	226.3
			0.095	45°	10	328.2	248.4
			0.127	45°	10	268.5	228.2
			0.159	45°	10	223.4	200.7
			0.127	$22\frac{1}{2}^{O}$	10	181.2	125.5
			0.127	33.8^{O}	10	235.6	187.7
			0.127	$56\frac{1}{4}^{O}$	10	283.4	249.8
			0.127	45°	100	414.6	352.4
Fe^{55}	Olivine	Si	0.127	45°	10	150.0	127.5
Cd^{109}	Olivine	Si	0.127	45°	1	15.0	12.8
			0.127	45°	10	41.6	35.4
			0.127	45°	100	77.3	65.7
		Fe	0.095	45°	1	7472	5656
			0.127	45°	1	5986	5088
			0.159	45°	1	4880	4385
			0.127	$22\frac{1}{2}^{O}$	1	2974	2059
			0.127	33.8^{O}	1	4467	3560
			0.127	45°	10	54,380	46,220
			0.127	45°	100	188200	160000

window need be near this minimum value only over the central portion which is irradiated by the primary x-rays. Near the rim it could thicken significantly to provide for easier attachment to the top of the support cone and increased strength. Spectral distortion produced by the thicker window could be reduced by operating the proportional counter at a lower pressure and providing an exit window for the harder secondary radiation not stopped by the counter gas.

3.2 DESIGN

Any absorbing medium attenuates soft x-rays more strongly than it does the higher energy radiations. As a consequence, the emergent spectrum is a distortion of the incident spectrum, the extent of the distortion being a function of the thickness of absorber and the wavelength range present in the spectrum.

Consider a typical olivine, $(Fe_{0.5}, Mg_{1.5})SiO_4$, and for simplicity assume that the secondaries come from the first layer of molecules. There are three times as many magnesium atoms as iron atoms, but the fluorescent yield for iron is 11.8 times that for magnesium. Consequently, the Fe line would be about 5 times as strong as the Mg line. When secondaries from deeper-lying layers of molecules are included, differential absorption in the olivine increases this ratio by an order of magnitude or more, depending upon the depth of the layer. To this will be added the distortion introduced by the beryllium windows which separate the fluorescing molecules or atoms from the gas of the proportional counter. If we (somewhat arbitrarily) take a factor of 25 as an acceptable distortion due to the beryllium, giving a total minimum distortion factor of 100, the window thickness is given by

$$t = \ln 25/(\mu_{Mg} - \mu_{Fe})$$

$$= 3.22/(454 - 4.3)$$

$$= 0.0072 \text{ cm } (7.2 \times 10^{-5} \text{ m})$$

$$= 0.0028 \text{ inch } (7.2 \times 10^{-5} \text{ m})$$

A more restricted range of x-ray energies could tolerate a thicker window while producing comparable distortion of the spectrum. Calculations are easily made using data from the table below which lists pertinent data for a number of elements likely to be present in Venusian dust. The primary x-ray source, Ag-109, is included for reference.

Element	$\lambda K\alpha$ Å	keV	(μ/ρ) Be	μcm^{-1}	$W_2 K\alpha$	Sp. Gr.
Na	11.91	1.04	418	773	0.025	0.97
Mg	9.89	1.25	246	454	0.029	1.74
Al	8.34	1.49	151	279	0.038	2.702
Si	7.13	1.74	96.2	178	0.043	2.33
P	6.16	2.01	63.3	117	0.060	2.35
S	5.38	2.31	42.9	79.4	0.082	2.07
Cl	4.73	2.62	29.8	55.1	0.097	3.214
K	3.75	3.31	15.2	28.1	0.14	0.86
Ca	3.36	3.69	11.2	20.7	0.16	1.54
Mn	2.11	5.89	2.9	5.4	0.313	7.20
Fe	1.94	6.39	2.3	4.3	0.342	7.86
(Ag)	(0.57)	(22.0)	(0.1)	(0.2)	(0.834)	(10.5)

Window thickness, as a limiting factor, is also significant for its effect on count rates. The data given at the end of Section 3.1.3 indicate that the thickness of the upper window is not particularly critical if one can assume a dust layer at least 1 micron (1×10^{-6} m) thick, and if the dust layer approaches 100 microns (100×10^{-6} m) in thickness, degradation of counter performance becomes a greater problem than the thickness of beryllium in the system. For these reasons, and because of the added

31

reliability introduced by redundancy, a dual experiment is proposed consisting of a small, thin hemispherical beryllium window with an Fe^{55} source, plus a larger, thicker hemispherical beryllium window with a Cd^{109} source. The first system will be able to analyze for elements with a Z range from 11 (Na) to 23 (V), and in principle the second system will be able to analyze for elements up to Z = 44 (Ru) though it is unlikely that many elements beyond iron will be present in measurable concentrations. This range of elements could be extended by analyzing for L-shell fluorescent radiations.

Each system will have the configuration of Figure 4 with a source supported on a spider as shown in Figure 3. The hemispherical window of the first system would have a minimum thickness of 0.006 cm (6×10^{-5} m) and an inside diameter of 0.20 cm (0.2×10^{-2} m). The source will be positioned approximately $0.9 \, r_2$ below the center of the window. The exact distance can only be determined after a detailed source-shield design has been completed. (A tentative source shield schematic is given in Figure 8.) The hemispherical window of the second system will have a minimum thickness of 0.025 cm (2.5×10^{-4} m) and an inside diameter of 1.0 cm (1×10^{-2} m). The lower window in each system will have a thickness of 0.003 cm (3×10^{-5} m). An exit window on the second proportional counter made of beryllium honeycomb sandwich is being tentatively considered.

A single calculation of C_i was made for a Cd^{109} source analyzing for Fe in olivine dust using the 1-cm diameter window, thickness 0.025 cm. The uncorrected count rate was $C_i = 7069$ per second for a dust layer 1 micron thick.
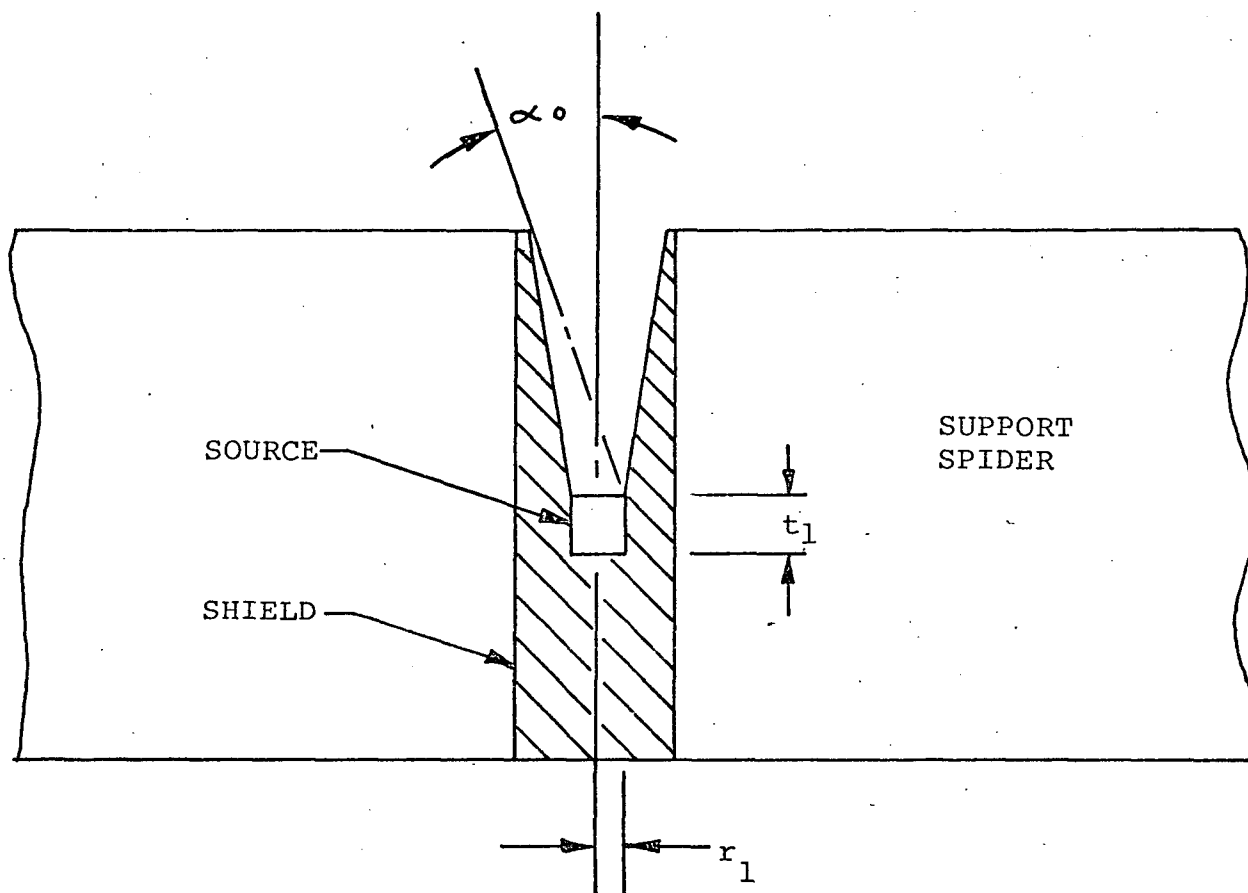
Figure 8. Source-Shield Geometry and Support
Spider in Cross Section

4.0 SYSTEM DESCRIPTION

This section presents an overall description of the proposed version X-RAY FLOURESCENCE ANALYZER and it covers specifications, configuration, data and mission requirements, and instrument power consumption. A detailed discussion of the electronics is given in Appendix A.

4.1 INSTRUMENT DESCRIPTION

The X-RAY FLUORESCENCE ANALYZER is an instrument for the quantitative analysis of Venusian dust and condensates. Samples collected on a beryllium window are illuminated by x-rays from a radioactive source, and the resultant characteristic fluorescent x-rays are detected and pulse height analyzed by a simple spectrometer. To provide better coverage of the elements of interest two detectors and sources with overlapping energy ranges are used. A single set of electronics serves both.

Figure 1 illustrates the proposed instrument. The identical cylindrical proportional counters are mounted outside the pressure vessel on a 2.5 inch square (16.12 x $10^{-4}m^2$) platform which is thermally isolated from the probe structure. On the counter body a sample window housing supports a thin concave beryllium foil window, transparent to the X-rays of interest. The counter, sample window housing and the sample window itself are capable of operating in the Venusian environment.

Inside the sample window housing, a soft x-ray primary source (Fe^{55} for low energy detector A and Cd^{109} for high energy detector B) irradiates the sample window as shown in the inset. Dust or condensed material on the window absorbs a fraction of the incident radiation (depending on sample thickness) and emits characteristic K x-rays. Some of these fluorescent x-rays pass through a second window into the gas filled proportional counter, where they are absorbed by the photoelectric process and converted to current pulses whose charge content is proportional to the x-ray energy. The pressure inside the

counter is only a few atmospheres even at 500° C (773°K) so that the counter window does not pose a serious structural problem. A relatively large, flat window is used to maximize the solid angle of collection.

A single shielded high voltage electrical connection is required by each detector. Braided fiberglass insulated wire inside a tubular metal shield is one possible configuration for this interconnection. It may be desirable to locate the electrical connections inside the detector supports.

The block diagram of Figure 9 shows the organization of the electronics required to process the counter output signals. Each counter has an associated high voltage bias supply (2 to 3 kV) and a signal processor. The signal processor contains a charge-sensitive preamplifier to cover the charge pulse to a voltage pulse, a post amplifier, and pulse height analyzer which measures the pulse amplitude and presents it as a digital number.

To minimize the data bandwidth required by the instrument, the analog-to-digital conversion transfer function of the pulse height analyzers is made nonlinear in such a way as to approximately match the detector resolution. Specifically, the analyzer resolution will be about one-tenth of the detector resolution (10 energy channels under a peak, measured at full width at half maximum). The ranges of the analyzers will be about 0.5 to 5 KeV for detector A to 1 to 10 KeV for detector B.

Outputs from both pulse height analyzers are fed into a common memory system on a pulse-by-pulse basis. For each possible digital number representing a pulse height (energy) there is a corresponding memory location in which is stored the nember of counts accumulated for that energy. Each time a pulse with that amplitude occurs, the count stored in the memory location is read, incremented by one count, and written back into the memory.

One quarter (128 channels) of the memory is devoted to accumulation of a spectrum from each counter as described. At the same time, data is being read out from the other half of memory to the prove telemetry system. A simple priority system time-shares memory operation between the three users (detector A, detector B, and telemetry). A memory cycle takes only a few microseconds, so that real-time access without appreciable delay is realized.

PROPORTIONAL
COUNTER A

FE-55 SOURCE

SAMPLE
WINDOW A

HIGH VOLTAGE A

CHARGE-
SENSITIVE
PREAMPLIFIER

POST
AMPLIFIER

PULSE
HEIGHT
ANALYZER

SIGNAL CONDITIONER A

ENERGY DATA A

PROPORTIONAL
COUNTER B

CD-109 SOURCE

SAMPLE
WINDOW B

HIGH VOLTAGE B

SIGNAL CONDITIONER B

ENERGY DATA B

MEMORY
SYSTEM

1 MHz
30-60 Hz CLOCK
FRAME PULSE
BIT CLOCK
WORD GATE
SERIAL DIGITAL
DATA

HOUSEKEEPING
CIRCUITS

4

ANALOG DATA

HIGH VOLTAGE A

HIGH VOLTAGE
POWER SUPPLY
A

LV POWER
TO ALL
CIRCUITS

LOW VOLTAGE
POWER SUPPLY

28 VDC ±2%

HIGH VOLTAGE B

HIGH VOLTAGE
POWER SUPPLY
B

FIGURE 9. BLOCK DIAGRAM

36

Because the thickness and composition of the sample is unknown, the count rate for the proportional counters is also uncertain. A wide dynamic range is provided by adjusting the accumulation time automatically (up to 10 minutes) to compensate for variations in count rate.

Telemetry data consists of 125 10-bit words of energy data per detector, one word per detector indicating accumulation time, and four synchronization and housekeeping words for a total of 256 data words (2560 bits) per data frame.

Computer analysis of the spectra will estimate the composition of the sample by unfolding techniques making use of data from pure elements and representative mixtures. A small amount of leakage of primary x-rays and/or fluorescent radiation from selected targets will provide in-flight calibration of system gain, linearity, and resolution using the normal instrument operating mode.

Although the detailed design of the instrument is specific to the Pioneer Venus mission, the experimental technique is highly developed and is routinely used in laboratory analysis of complex materials. Proportional counter x-ray spectrometers, some using radioactive sources, have been designed and/or flown on many spacecraft, including OGO, OSO, Apollo and Viking. The electronics proposed is straightforward and employs proven techniques. Laboratory studies by the investigators have verified the fundamentals of the experiment and established the feasibility of analyzing dust layers a few tens of microns thick. Further studies during the experiment definition phase will optimize the detector and source design and verify the environmental integrity of the detector assembly.

Table II gives the physical, electrical, data, and environmental specifications for the X-RAY FLUORESCENCE ANALYZER.

TABLE II

X-RAY FLUORESCENCE ANALYZER SPECIFICATION SUMMARY

Physical Parameters

Weight	4.9 lb (2.2 kg)
Volume	168 cu in (2.75 x 10^{-3} m^3)

Dimensions

Detector	2.5 x 2.5 x 2 inches (6.35 x 6.35 x 5.08 x 10^{-2} m)
Electronics	7 x 8 x 3 inches (17.78 x 20.32 x 7.62 x 10^{-2} m)

Electrical

Input Voltage	28 Vdc ±2 percent
Power	2W (constant)
Power Duty Cycle	Continuous

Timing Signals

PHA and Memory	1 MHz and 30-60 Hz clocks
Data	Bit clock, word gate, frame pulse

Output Signals

Digital	Serial digital data
Analog (four)	2 high voltage, 1 low voltage, and 1 temperature monitor

Data

Data Frame Length	2560 bits
Readout Rate	Arbitrary
Readout Cycle	10 minutes nominal
Average Data Rate	4.3 bps nominal

Commands

None required -- activated by power turn-on.

Operational Cycles

One operating mode -- internally timed data cycle.

Deployment Mechanisms

Ejection of dust cap required.

Environmental Constraints

Detector	100 bar (1 x 10^5 N/m^2), $-40^{\circ}C$ ($233^{\circ}K$) to $500^{\circ}C$ ($773^{\circ}K$)
Electronics	1 bar (1 x 10^5 N/m^2), $-40^{\circ}C$ ($233^{\circ}K$) to $60^{\circ}C$ ($333^{\circ}K$) non-operating; $-20^{\circ}C$ ($253^{\circ}K$) to $50^{\circ}C$ ($323^{\circ}K$), operation within spec
Electromagnetic	Normal spacecraft EMI constraints

4.2 INSTRUMENT CONFIGURATION

The general configuration of the X-RAY FLUORESCENCE ANALYZER was described in the previous section. Refer to Figure 1 for a sketch of the instrument. Specific configuration data follows.

(a) Envelope. The overall dimensions of the detector assembly are 2.5 x 2.5 x 2 inches (6.35 x 6.35 x 5.08 x 10^{-2}m). Mounting provisions and connector locations shown in Figure 1 are tentative. It is assumed that the spacecraft contractor will provide the coaxial feedthrough connectors and assist in the design of the thermal isolation/support details.

The electronics assembly is housed in a rectangular package 7 x 8 x 3 inches (17.78 x 20.32 x 7.62 x 10^{-2}m). It should be located within a short distance (preferably 6 inches)(15.24 x 10^{-2}m) of the detector feedthrough to minimize the possibility of electromagnetic interference. The form factor of the electronics package can be modified if necessary, and it can be mounted on any face. In addition to the two high voltage coaxial detector connectors, a probe interface connector and a test connector are required.

(b) Weight and Volume. A preliminary estimate of the weight of the X-RAY ANALYZER is summarized in Table III. As indicated, the total weight for detector and electronics is 4.9 lb (2.2 kg).

Based on the dimensions mentioned above, the instrument volume is 168 cubic inches (2.75 x 10^{-3}m^3).

4.3 INSTRUMENT POWER

Internal analog circuits of the X-RAY FLUORESCENCE ANALYZER require ±5 Vdc and ±10 Vdc regulated to ±2 percent over line, load, and temperature variations. The +10V line will also be used to power CMOS memory and logic circuits, as these require very little power. The two high voltage power supplies for detector biasing require 28 Vdc ±5 percent, isolated from the probe power bus.

Due to the potential noise susceptibility of signal conditioning circuits, it is preferred to generate all low voltage power internally from a dc-to-dc converter within the experiment, although regulated spacecraft

TABLE III

WEIGHT ESTIMATE

Item	Weight	
Detectors	200	
Detector Mount	60	
Interconnect Cables	40	
Subtotal	300	300
Detector Assembly		
Discrete Components	570	
Integrated Circuits	100	
Printed Circuit Boards	280	
Connectors and Wiring	140	
Bonding and Potting	220	
Housings and Covers	540	
Hardware	70	
Subtotal	1920	1920
Electronics Assembly	Total	2220 g (4.9 lb 2.2 kg)

power is an alternative. A regulator will remove line voltage variations and provide current limiting.

Power consumption will be virtually constant. An increase of less than 1 percent is predicted as the detector count rate increases from zero to maximum. A breakdown of the instrument power requirements is given in Table IV.

4.4 INSTRUMENT DATA

The X-RAY FLUORESCENCE ANALYZER will have only one operating mode. Calibration is automatically accomplished during operation by allowing a small fraction of the source x-rays and fluorescence x-rays from selected targets to leak into the detectors.

X-ray data will be in the form of a data frame consisting of 256 10-bit data words. The data frame will contain three synchronization words, one housekeeping word, one detector 1-time word, 125 words of detector 1 data, one detector 2-time word and 125 words of detector 2 data. This format is shown in Figure 10.

If the readout of the data frame is accomplished in 10 minutes, the average bit rate will be 4.27 bps. The readout period is not critical and could be increased or decreased by a factor of two without affecting instrument objectives.

Instrument readout circuits can be designed to accommodate virtually any data system interface requirements. For preliminary estimates, a serial digital telemetry system controlled by a shift clock and word gate has been assumed. Telemetry bit rates up to 1 MHz with any word length are acceptable. A telemetry frame pulse occurring once (or a few times) per data frame is also required for synchronization.

Operation of the analyzer requires two timing signals of approximately 1 MHz and 30 to 60 Hz for PHA timing and accumulation timing, respectively. It is assumed that the probe will provide these frequencies or convenient multiples.

Only a power turn-on command is required from the probe. All other sequencing will be internally controlled.

TABLE IV

INSTRUMENT POWER SUMMARY

Circuit	Quantity	Power/Unit	Total
High Voltage Power Supply	2	150 mW	300 mW
Signal Conditioner	2	75	150
Pulse Height Analyzer	2	350	700
Memory System	1	.20	20
Housekeeping Circuits			100
Reserve			100
Total Conditioned Power			1370 mW
Low Voltage Power Supply			580
Total 28V Power			1950 mW
			(1.95W)

```
WORD                CONTENTS

  1    |         SYNCH 1            |
  2    |         SYNCH 2            |
  3    |         SYNCH 3            |
  4    |   DIGITAL HOUSEKEEPING     |
  5    |        DET 1 TIME          |
  6    |        DET 1 CH 1          |
  7    |        DET 1 CH 2          |
  8    |        DET 1 CH 3          |

130    |        DET 1 CH 125        |
131    |        DET 2 TIME          |
132    |        DET 2 CH 1          |
       |        DET 2 CH 2          |

256    |        DET 2 CH 125        |
```

Figure 10.   X-Ray Fluorescence Analyzer
              Data Format

43

Depending on the detector cable and connector design, it may be desirable to delay turn-on of the instrument until the pressure has reached a few hundred millibars.

The analyzer detectors and the cables between the detectors and electronics will be designed to provide shielding against RF interference. Standard EMI requirements imposed on instrument/spacecraft interfaces will be adequate to prevent degradation of instrument performance.

4.5 INSTRUMENT ENVIRONMENTAL CONSTRAINTS

The detector assembly will be designed to withstand the Venusian surface temperature and pressure of 500°C (773°K) and tests performed to verify that the thin beryllium sample window will safely endure these conditions. A cylindrical counter configuration with metal end caps was chosen to provide a rugged pressure vessel within which the detector entrance window, anode insulators and similar parts can be mounted using conventional techniques. Operation of the detector at high temperatures is an area requiring investigation during the experiment definition phase. Although proportional counters are relatively stable over ordinary temperature ranges and no mechanisms precluding operation at 500° C (773°K) are known, the unusual conditions of the mission present a unique environment and verification of detector design and performance is essential.

4.6 SPACECRAFT INTERFACES

As discussed above, the X-RAY FLUORESCENCE ANALYZER has thermal and electrical interfaces with the spacecraft. The detector assembly should be located under the heat shield and the detector windows must be covered with a dust-tight cap which is discarded with the heat shield or jettisoned later. The dust cap will also act as a radiation shield for the x-rays. For the present it is assumed that the dust cap design will be accomplished by the spacecraft contractor.

Aerodynamic studies during the experiment definition phase will establish the preferred location for the detector assembly for optimum dust collection efficiency.

44

4.7 SPACECRAFT MISSION REQUIREMENTS

The X-RAY FLUORESCENCE ANALYZER is non-critical with respect to mission constraints. However, measurements should be made from a few hundred millibars to the surface. Primary emphasis is on the region near the surface, where dust concentration can be expected to be high and most representative of the surface itself. No changes in spacecraft attitude or instrument sensing direction are required, but such changes will not conflict with the experiment objectives.

4.8 PRE-LAUNCH SUPPORT REQUIREMENTS

The X-RAY ANALYZER is unusual in that operation of the instrument can be checked by merely observing leakage from the primary sources and/or fluorescence from the dust cap or other suitable target. Preliminary installation and checkout requirements consist primarily of verifying spacecraft mechanical, thermal and electrical interfaces, as well as the normal environmental test sequences. Facility requirements are limited to bench and office space for one or two experiment personnel. No special test equipment is needed, except for bench test equipment to simulate the spacecraft interface and collect and display instrument data. A laboratory pulse height analyzer for independent verification of detector performance is also required. No services other than 115 Vac power for test equipment are necessary.

4.9 FLIGHT OPERATIONAL REQUIREMENTS

No operational requirements for control or execution of the experiment exist.

4.10 DATA SUPPORT REQUIREMENTS

Computer analysis of data prior to reduction by the investigators is limited to decommutation and formatting of the instrument data and correlation with independent time and attitude information. Vehicle attitude versus time may also be useful in the interpretation of data in terms of dust concentration using aerodynamic analysis.

It is desirable that data be provided to the investigators on magnetic tape in a form suitable for further processing by a computer.

5.0 SUMMARY

This section provides an overview of the work performed on this study project, an evaluation of the proposed X-RAY FLUORESCENCE ANALYZER, and recommendations related to implementation of a hardware development project.

5.1 REVIEW OF PROJECT RESULTS

The counter tube window and X-RAY FLUORESCENCE ANALYZER study was conducted over a 6-week period. It covered theoretical analyses, conceptual development of the ana·lyzer, and design of the detector and electronic assembly configurations to the component level.

Special emphasis was placed on the window design, which represents the most critical element in the analyzer system. Two aluminum mockups were fabricated to illustrate the configuration of the proposed design.

Spacecraft considerations were also examined to assure compatibility of the analyzer and spacecraft. Instrument power, weight, and data requirements were defined. In addition, the X-RAY FLUORESCENCE ANALYZER was evaluated in terms of mission, pre-launch support, and flight operational requirements.

A cost estimate for the entire project was also prepared. This estimate is given in Appendix E. A project schedule was formulated for the development, fabrication, and test of prototype and flight models. (See Appendix C.)

5.2 EVALUATION OF PROPOSED DESIGN

The design described in the preceding sections will result in a compact, low-weight instrument that will reliably collect data on the characteristics of Venusian dust and condensates. It is expected that dust layers in a wide range of thicknesses will be measured. By optimizing the window configuration and designing the electronics to accommodate a wide range of count rates, dust layers of any thickness greater than 0.1 micron (1×10^{-7}m) thick can be detected.

46

Simplicity, reliability, and high performance are key features of the analyzer design. It is completely self contained, except for the spacecraft power source and consists of two packages: the detectors and electronics. Single-sided, double-sided, and multilayer printed wiring boards will be used to attain the most compact and reliable packaging configuration. Standard established-reliability parts will be used for most of the analyzer. However, some new memory integrated circuits will be used because of their low power requirements. These will be subjected to qualification tests before use in the flight analyzer.

The detectors for the analyzer will have to be developed because existing components cannot provide the desired performance. This phase of the project will require a special effort to fabricate and evaluate the windows and detectors. It is expected that the preceding design configuration will require some redesign to obtain the best flight configuration.

5.3 RECOMMENDATIONS

The incorporation of an X-RAY FLUORESCENCE ANALYZER on the Pioneer spacecraft will provide exceptionally valuable data on the characteristics of the Venusian surface dust in the atmosphere. This data will supply researchers with a basis for analyzing the composition of the planet's surface.

The detector-window represents the first priority area in design and development of the X-RAY FLUORES-CENCE ANALYZER. Work should begin on this right away to assure complete design and evaluation of the windows and associated detectors. Fabrication of the windows from beryllium also represents a potential problem area because of its mechanical properties which may involve special machining. Although the window and detectors require a special development effort, the results of the study indicate that both components are within the state of the art and that they can be successfully developed within the Venusian Pioneer program schedule.

APPENDIX A

DETAILED ELECTRONICS DESCRIPTION

The description of electronic circuits in the X-RAY FLUORESCENCE ANALYZER is based on circuits previously developed for other spaceborne applications. For this application, the circuits will be suitably changed or modified as requirements dictate. Improvements in the state of the art of circuitry as well as the latest improved hardware will be used in all instances to assure optimum performance and minimum power drain.

A tentative list of components based on the designs mentioned is given in Appendix F.

A.1 GENERAL

The X-RAY FLUORESCENCE ANALYZER consists of two essentially identical channels feeding into a memory system, plus a power system that supplies all necessary voltages for operation. Each analysis channel consists of a proportional counter (detector), signal conditioner, and pulse-height analyzer.

The detector is a proportional counter, which will be designed for this system. Output from the detector is a current pulse with a charge content proportional to the energy content of radiation incident on the detector. A signal conditioner, consisting of a charge-sensitive preamplifier and a post amplifier, changes the current pulse to a voltage pulse of the proper shape to minimize noise and offer easiest analysis. A pulse-height analyzer (PHA) then detects the maximum pulse amplitude, digitizes it, and stores the digital energy value in a memory.

A.2 SIGNAL CONDITIONER

A.2.1 Charge-Sensitive Preamplifier

The charge-sensitive preamplifier is shown in Figure A-1. High voltage is fed to the detector through a

+HV

DET
LOAD

FROM
DET

TEST

+V

TYPICAL
IMPLEMENTATION

R_f

C_f

V REF

I

OUTPUT

49

+HV

FROM
DET

TEST

C_f

R_f

−K

OUTPUT

FUNCTIONAL
DIAGRAM
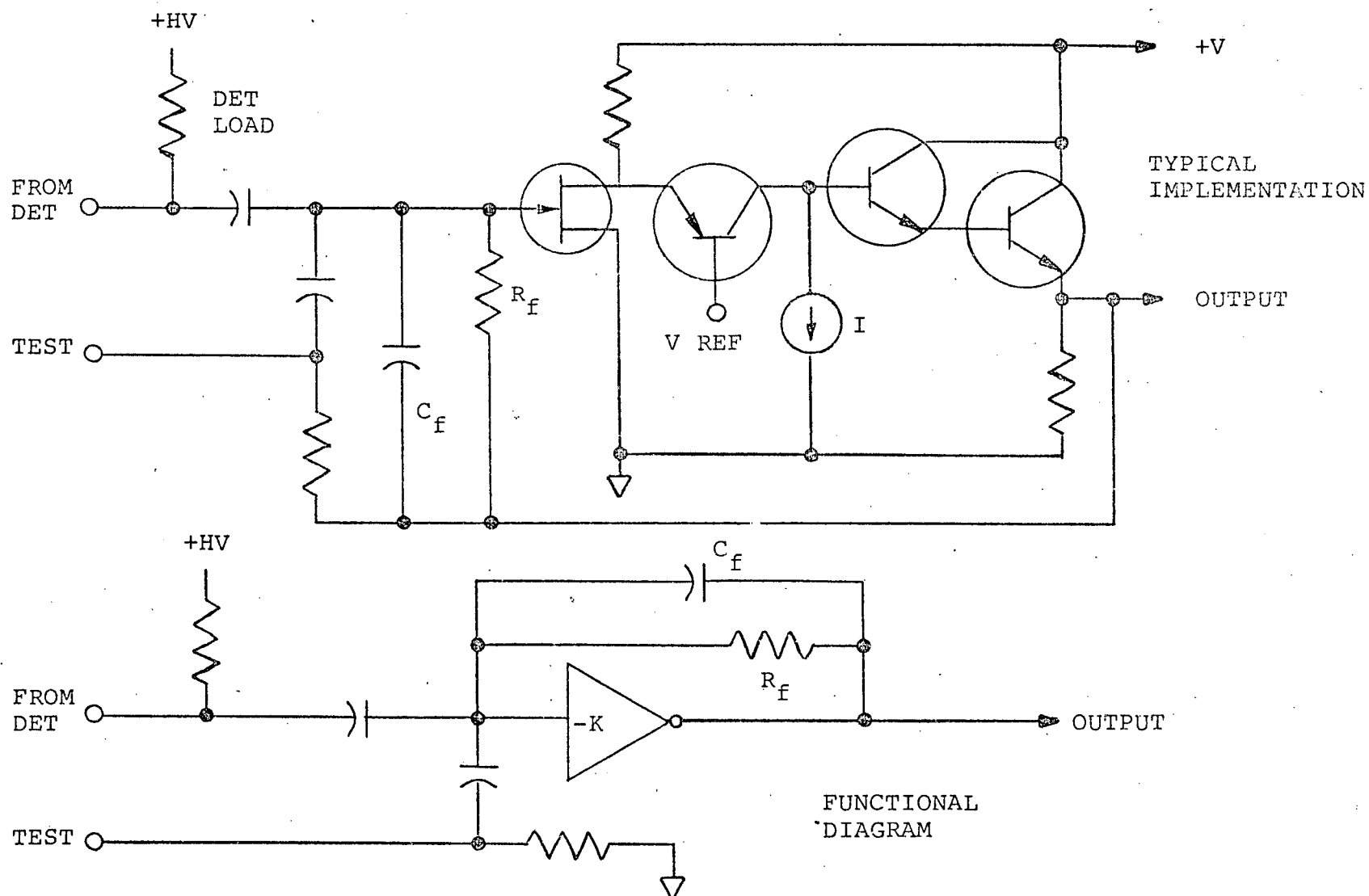
Figure A-1. Preamplifier

load resistor, and the detector is coupled to the preamp by a capacitor into the input FET. This FET, as are all the components of the preamp, is selected for very low noise.

When the detector fires, current is drawn through feedback capacitor C_f. As can be seen from the functional diagram, capacitor C_f feeds back from the amplifier output to integrate the pulse. This determines the amplitude of the amplifier output pulse since $V_{OUT} = Q/C_f$, where Q is the charge content of the pulse and is proportional to energy. Resistor R_f determines the discharge characteristics of the pulse.

Because the input FET has a relatively high output impedance, a pair of transistors is connected as a Darlington emitter follower to provide a very low output impedance to drive C_f, R_f, and the following post amplifier. Since the emitter follower does not invert, the phasing is not changed. Further amplification and level translation are gained through the use of a grounded-base transistor and a constant-current source, again without changing the phasing. Only major components are shown in Figure A-1.

A test input is supplied, consisting of a resistor to ground and a capacitor to the FET base. Detector simulation and electronics calibration can be accomplished by connecting a precision voltage tail-pulse generator to this input.

A.2.2 Post Amplifier

A post amplifier provides further gain as required, but its most important function is shaping of the pulse to reduce noise and to make it more suitable for the system characteristics. Shaping consists of double differentiation and double integration and is usually accomplished in two stages. Here, the same thing is accomplished in one stage by appropriate input and feedback RC networks as shown in Figure A-2.

The preamp inverts the detector signal and produces a positive pulse. The post amplifier also inverts so its output is a negative-going pulse. A second stage of inversion is therefore included to again provide a positive output to the pulse analyzer, and is also a handy place to set the channel overall gain with minimum effect on the waveform.

50

FROM
PREAMP

TYPICAL
IMPLEMENTATION

FROM
PREAMP
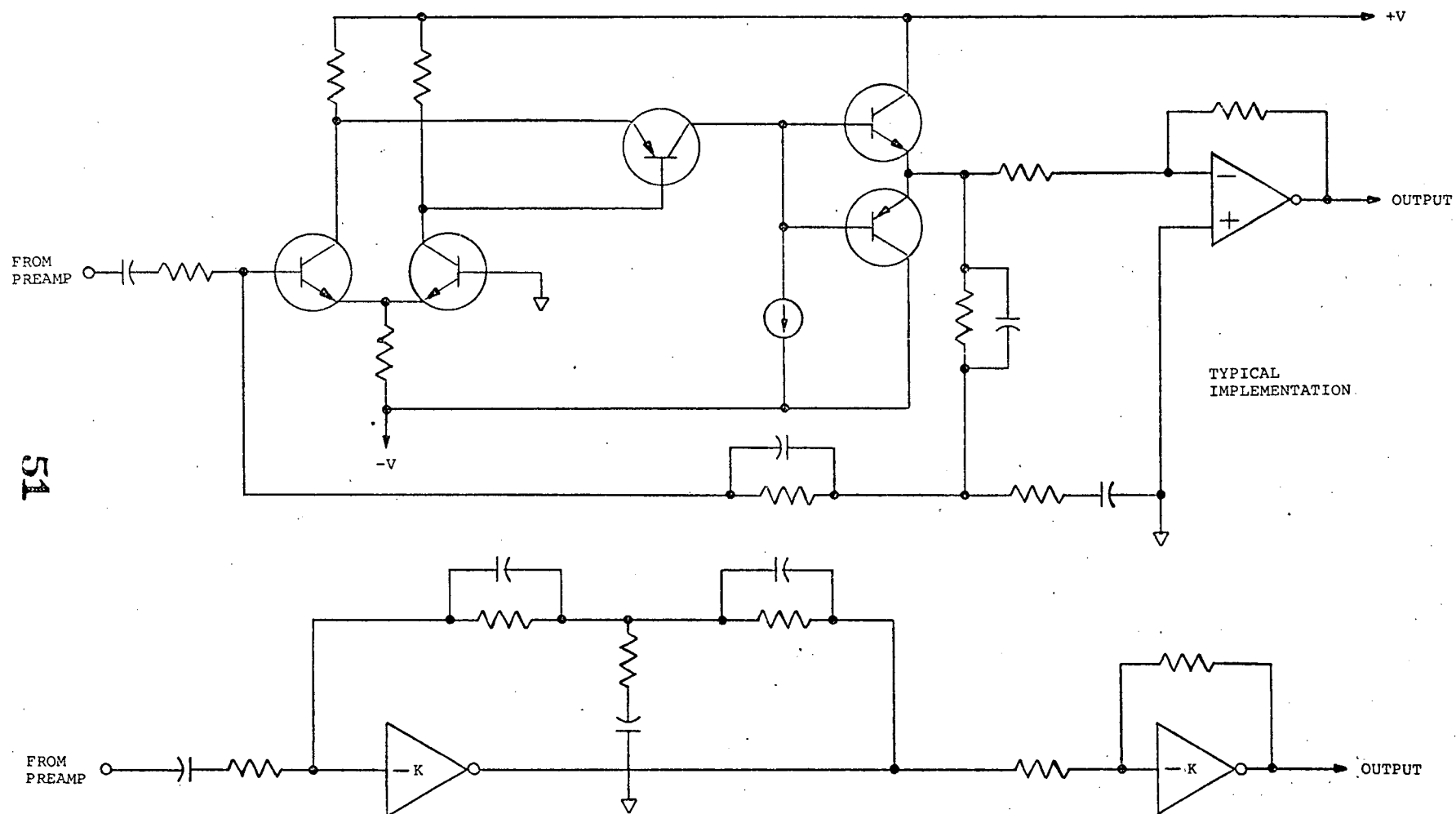
Figure A-2. Post Amplifier, Functional Diagram
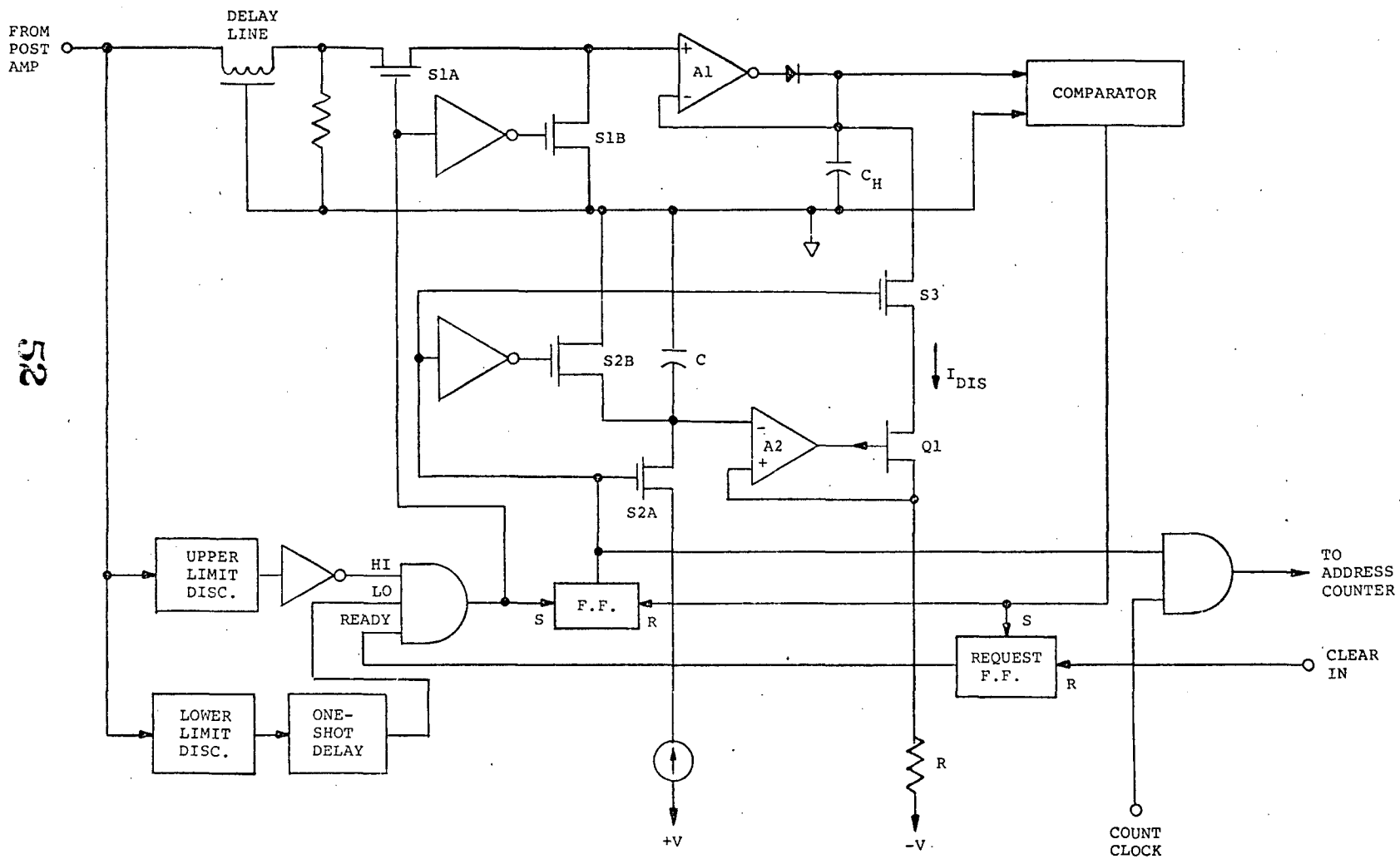
Figure A-3. Pulse Height Analyzer

A.3 PULSE-HEIGHT ANALYZER

Once a properly shaped pulse is available, it can be analyzed for height and that height (amplitude) turned into a digital number representing it. In Figure A-3, a few components are shown schematically while others are shown only functionally. The amplifiers are low-power integrated circuits that have been designed specifically for such applications. Logic symbols are standard, and the marked switches are transmission gates that are part of the COS-MOS logic series. This type of logic is used because it has the lowest power dissipation of any available -- literally micropower logic.

An input pulse from the post amplifier is applied directly to two discriminators. These are circuits that maintain one logic state at their output until the input signal exceeds a preset reference voltage, and then switch rapidly to the opposite logic state. A lower limit is set to determine the minimum energy to be analyzed and to exclude noise. As soon as the pulse exceeds this lower limit, the lower discriminator fires and provides a ONE output. A short time delay is furnished by a one-shot so that the change in logic level won't get to the gate until after the upper-level discriminator has had time to make a decision. If the pulse exceeds the upper energy level desired for the analyzer, a veto is provided by the upper discriminator to prevent the analysis.

If the pulse is within the energy limits desired, both outputs to the gate will be high (ONE) and the gate will trigger the circuit if the ready line is also high. The ready line will be high if analysis of the preceding pulse has been completed. An output from the gate closes S1A to connect the delay line to the peak detector. This signal through an inverter also opens S1B to remove the ground from the peak detector.

As the pulse rises, it successively triggers the lower discriminator, the upper discriminator (if too large), and reaches a peak. Since the peak is the value of interest, it must be delayed until after all decisions have been made as to whether or not to analyze. The delay line accomplishes this with little or no degradation of the pulse shape.

The peak detector consists of A1, the diode, and capacitor C_h. The amplifier is connected as a follower to the pulse signal. The diode is inside the loop so any

drop it might cause is divided by the open-loop gain of
Al. As long as the pulse is increasing in the positive
direction, the amplifier charges C_h to the value of the
pulse. As soon as the pulse falls below its peak, the
diode opens and the capacitor simply holds its charge.

The particular mechanism of digitizing the voltage
on the capacitor can take many forms. For this app-
lication, a technique is used that provides a nearly
constant resolution for the analyzer (see appendix D).
Once charged to its peak value, the capacitor is dis-
charged by a ramp current while a gate is opened to a
counter and clock. When the capacitor reaches zero, a
comparator turns off the gate, stopping the count and
providing a digital number representing the energy
content of the pulse.

When switch S1 is operated by the gate output, the
timing flip-flop is not triggered. However, when the
pulse starts its decay -- leaving its peak value on C_h --
the gate output will fall, triggering the flip-flop and
disconnecting the delay line through S1. The flip-flop
opens S2B and closes S2A and S3, and opens the gate to
let clock pulses be counted by the counter. Until now, C
has been shorted to ground and carries no charge. Now,
however, C is charged by the constant-current source and
develops a voltage in a linear fashion. This voltage
also appears at the upper end of R because of the follower
action of A2 and the P-channel FET, Q1, developing the
ramp current.

Limit Discriminator

Limit discriminators are conventional and can be
obtained in integrated-circuit form. For this application,
the power considerations outweigh size and a discrete
version, Figure A-4 is contemplated. It consists of a
differential amplifier, one side for signal and the other
for the reference level. A dual NPN transistor with a
current source in the common emitter lead provides the
majority of the gain. It drives a dual PNP transistor
that provides some additional gain but primarily provides
single-ended output as well as level translation of the
output voltage. Crossed diodes on the NPN collectors
limit the swing to the PNP to prevent saturation and
excessive recovery time. A conventional one-shot is
triggered by the sharp change in amplifier output to
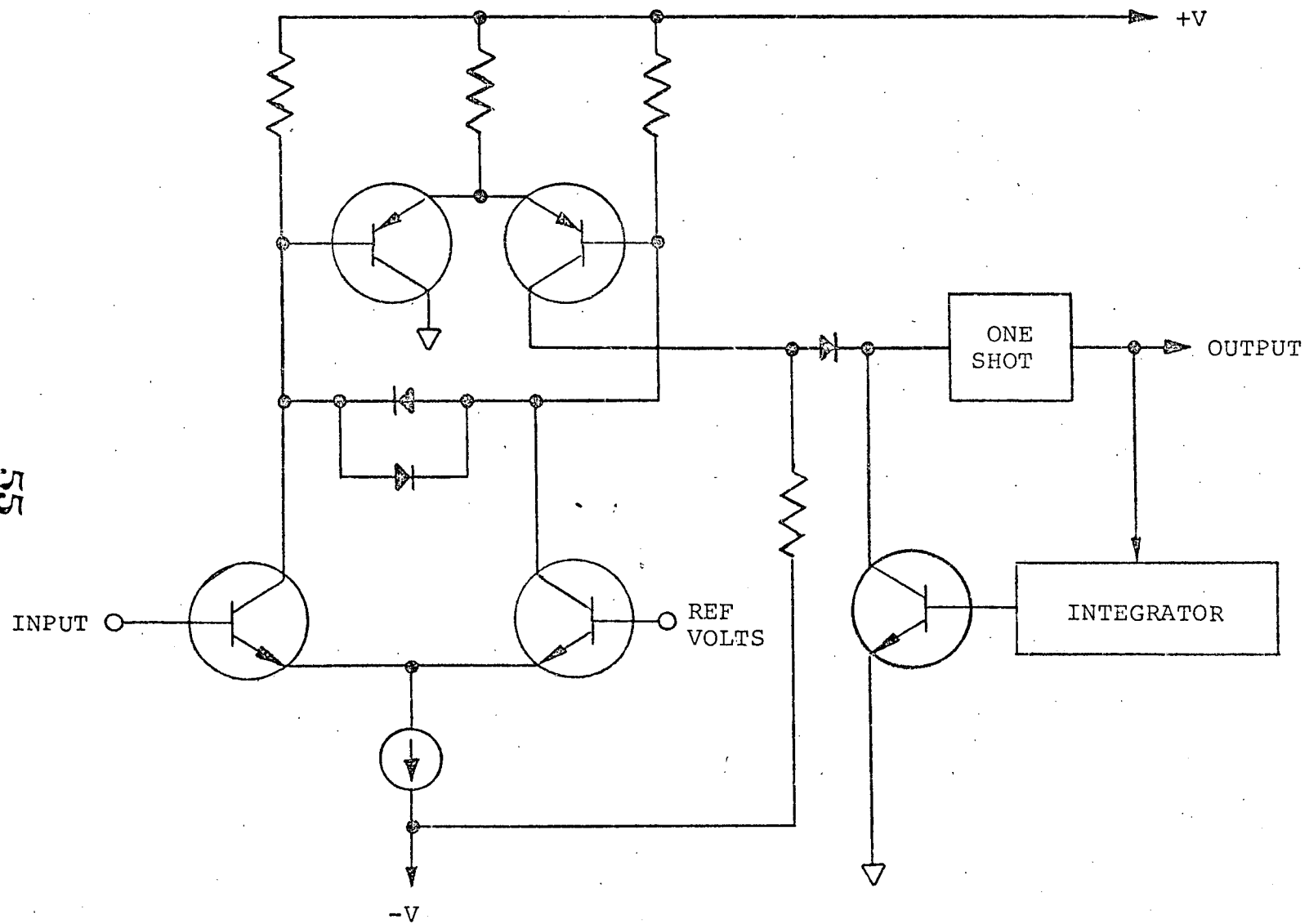
Figure A-4. Limit Discriminator

provide a signal to the following gate (or inverter).
The period can be preset so as to assure proper action
into the switches and flip-flop of the analyzer, without
depending on decay of the pulse. A transistor switch
fed through an integrator clamps the one-shot input for
a slightly longer period so that the discriminator cannot
be retriggered by another pulse during the one-shot period.

The comparator is simply a version of the dis-
criminator amplifier using a FET front end and omitting
the one-shot. Its output is intended to stay in one
state or the other, depending on input conditions.

A.4   POWER SYSTEM

The power system is of critical importance because
low power is an major objective and low generated noise
is a requirement for proper system operation.

A.4.1 Low-Voltage Power Supply

Space power supplies operate from sources that vary
perhaps ±2 percent in voltage, so a pre-regulator is
included to keep the voltage constant and to reduce surge
current and EMI. This consists of a straightforward series
regulator and current limiter and is not shown in detail.
A series regulator was selected instead of a switching
regulator so as to minimize noise fed back to the space-
craft source and noise in the system.

Basically, a power supply of this type consists of
a chopper or full-wave switch to change the incoming dc to
a square wave. This is fed to a transformer, which pro-
vides the necessary secondary voltages. The square-wave
output voltages are rectified and filtered for system use.
Commonly, the chopper is self-excited, using a saturating
transformer. Such an arrangement uses a minimum number
of parts but produces a large amount of noise. This
supply uses a non-saturating transformer and a separate
excitation for the chopper. Again, usually, the separate
excitation is another saturating transformer. Here,
however, a different scheme is used to keep the noise to a
minimum.

A simple astable multivibrator provides a square
wave at a predetermined frequency. This could be used
directly to excite the chopper transistors but such an
arrangement does not necessarily prevent overlap of the
chopper switching cycles, which is the chief source of

56
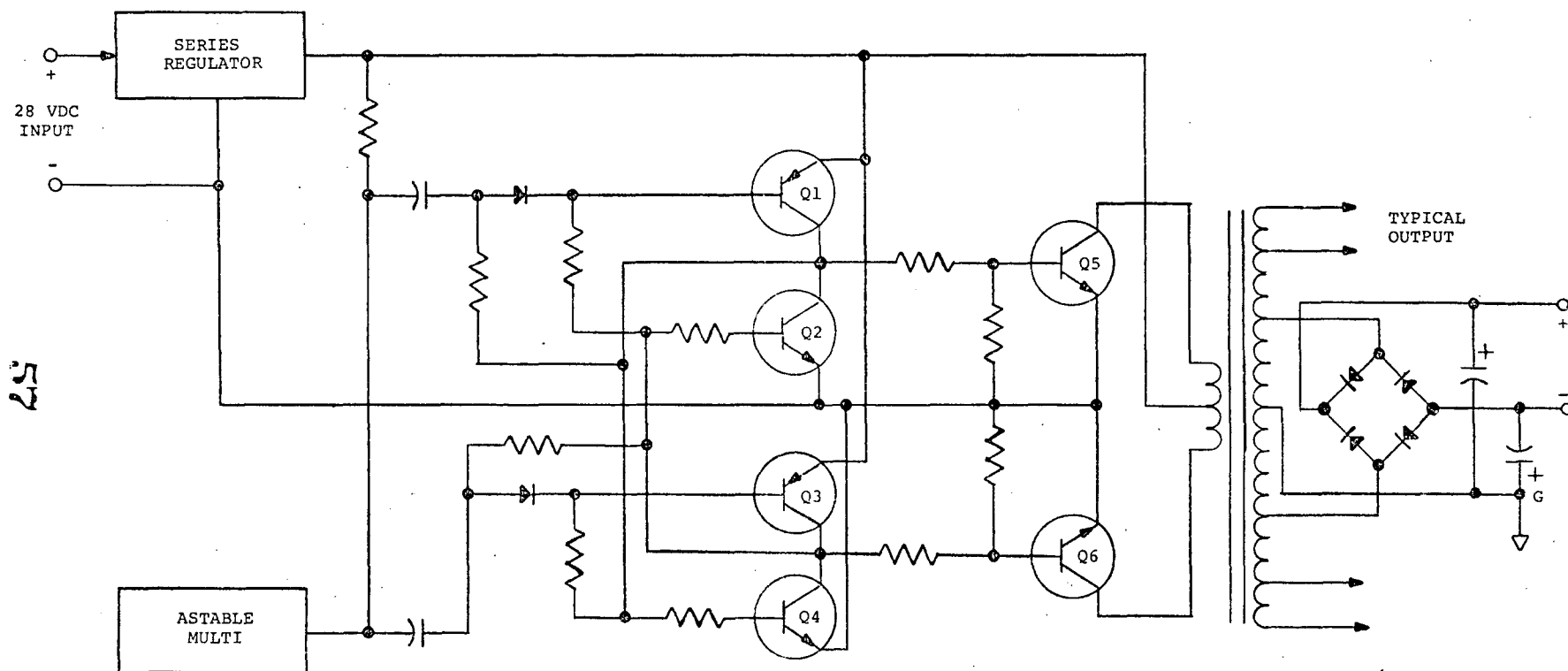
Figure A-5. Low Voltage Power Supply

LV INPUT

ASTABLE MULTI

VOLTAGE-CONTROLLED ONE-SHOT

+ HV

+

− O REF

COMPARATOR
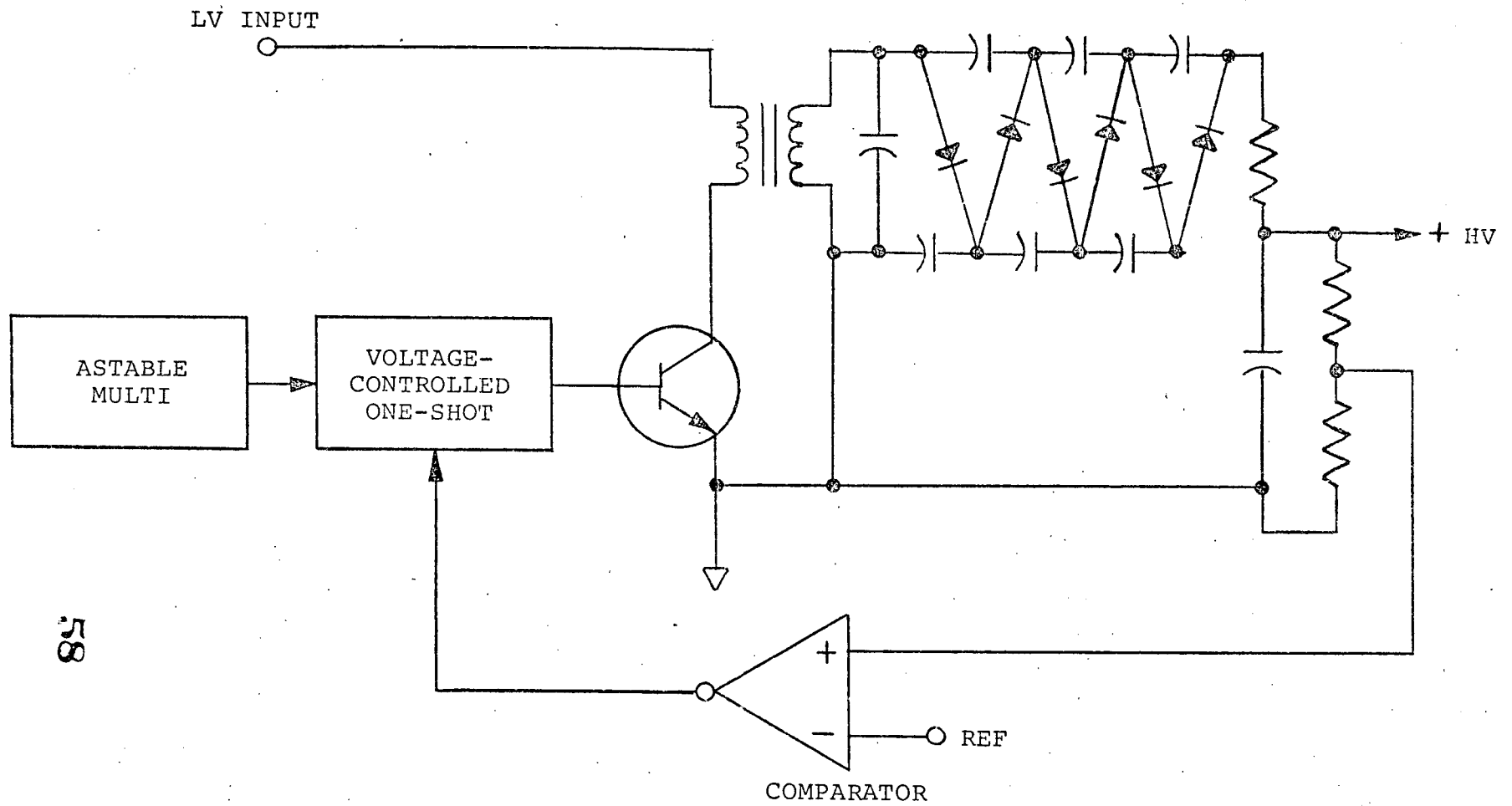
58

Figure A-6.   High Voltage Power Supply

noise. The circuit shown, consisting of two very fast NPN transistors and two PNP transistors, supplies square-wave drive to the chopper transistors without any overlap in time.

The technique is to switch ON an NPN, depriving a driven chopper of its base current to turn it OFF. Subsequently, through switching action in the slower PNP, current is supplied to the opposite chopper to turn it ON. Each positive transition of the astable causes this sequence alternately to the two choppers.

The remainder of the low-voltage supply is conventional, with each pair of outputs being rectified and filtered. Further noise filtering is taken care of by L-C filters in each output lead at the wall of the power supply housing. Although a bridge rectifier is shown, the transformer is center-tapped and the bridge acts simply as two full-wave rectifiers. Each of the other pairs of outputs is treated in a manner similar to that shown.

A.4.2 High-Voltage Power Supply

Two separate high-voltage supplies provide power to the two detectors, permitting separate adjustment and a degree of redundancy. Each consists of a transformer, astable, voltage multiplier, comparator, and a voltage-controlled one-shot for voltage regulation.

The astable is conventional. It cannot be the same one used in the low-voltage supply because that one is on the primary side of its transformer and is tied to the spacecraft power. DC for the high-voltage supply comes from one output of the low-voltage supply and is therefore isolated from the spacecraft.

The transformer sees a rectangular wave from alternate actions of the switching transistor. The secondary feeds a conventional voltage multiplier to provide an output of nominally 2 to 3 kV for its detector. A portion of the output is fed back to a comparator, which controls the one-shot duty cycle.

When the transistor switch is turned on, the transformer primary current increases at the rate of $di/dt = V/L$, where L is the primary inductance. At the instant the switch opens, energy stored in the transformer is $W = Li^2/2 = V^2t^2/2L$, where t is the ON time. This energy is transferred to the voltage multiplier by the transformer secondary to develop the output voltage.

If the output voltage is correct, the duty cycle will stay constant. If the voltage goes up, the duty cycle goes down and the output voltage is reduced. Similarly, a decrease in voltage causes an increase in duty cycle. As a result, the output voltage is held constant.

The one-shot is fairly conventional, using either a transistor or FET as a controllable current source in the base of one transistor to control the timing.

A.5   MEMORY SYSTEM

A.5.1   Memory

Figure A-7 shows the over all memory system. Central to the concept is an integrated-circuit memory comprising 32 IC chips. Each is a fully-decoded 256-address memory for one bit. However, as shown in Figure A-8, these chips are arranged as two separate 256x16 bit memory halves used alternately. During a given readout period, which is assumed to be 10 minutes, memory half A will accumulate data while memory half B will be read out to the spacecraft. During the succeeding period, the two memory halves will trade places, B accumulating and A reading out.

The half-select inputs activate the chip enable (CE) inputs for memory operation when desired. Except during a specific memory operation, neither input is enabled. Read-write (R/W) inputs are common to all chips; address inputs (8) to each chip are bussed to their same inputs on all chips. Data inputs and outputs are individual to each bit.

Also shown in Figure A-8 is a circuit for entry of memory output data into one flip-flop of the 16-bit register. Data entry is achieved when memory output is available and the reset-control line is low. If no data is available, the flip-flop will be reset.

60

Figure A-7. Memory System

61

8-BIT ADDRESS

READ-WRITE

HALF SELECT

R/W 256 x 16

CE

Ⓐ

DATA OUT

HALF SELECT

R/W 256 x 16

CE

Ⓑ

HALF SELECT

DATA IN

MEMORY ORGANIZATION
(1 BIT)

DATA IN

S Q

F.F.

R

OUTPUT

RESET-CONTROL

DATA ENTRY TO TYPICAL 1-BIT
STAGE OF 16-BIT REGISTER

62
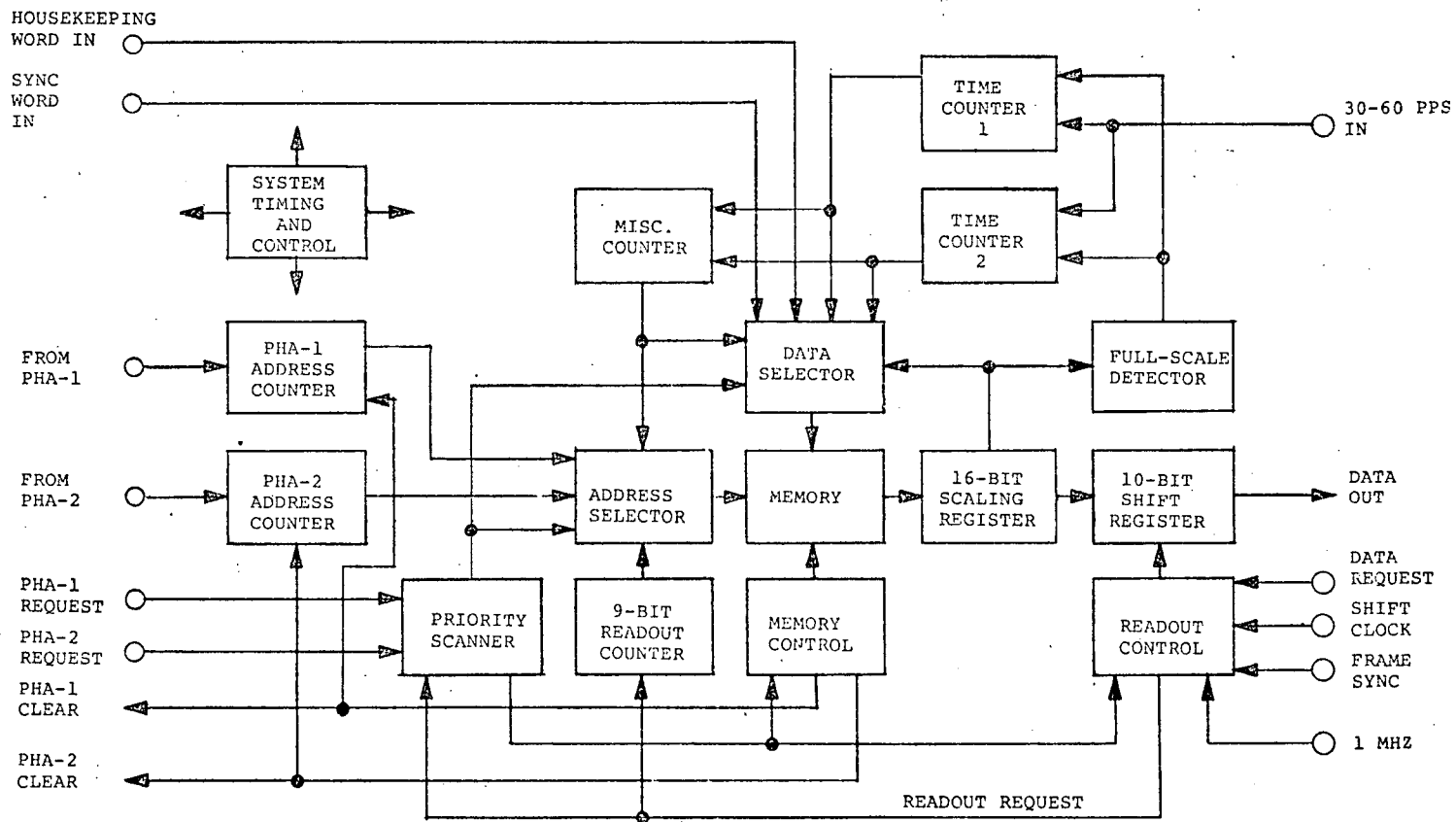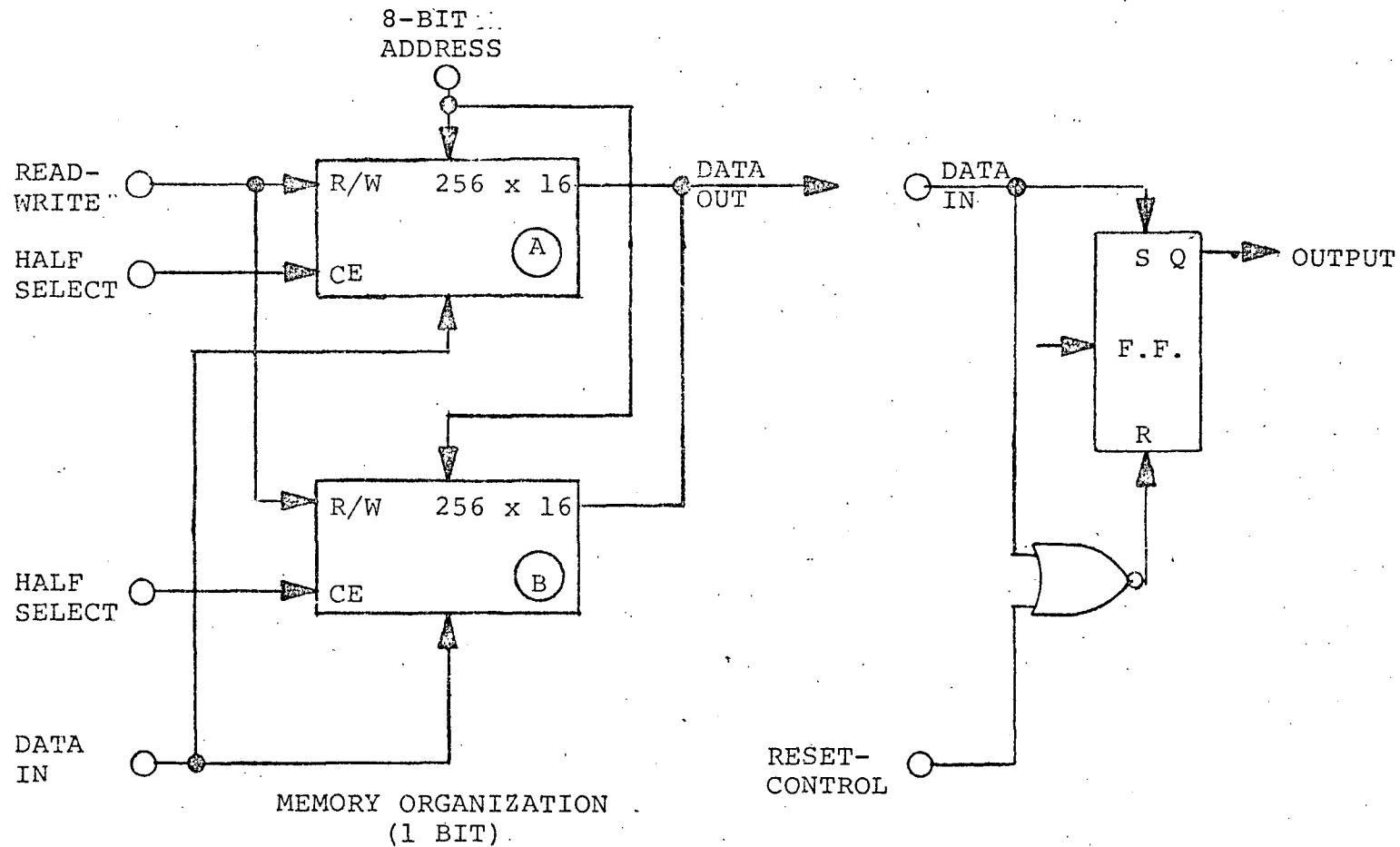
Figure A-8.   Memory Detail

A.5.2 Scaling Data Register

The data format comprises 7 data bits plus 3 code bits; the code bits determine how many prescaling flip-flops are inserted ahead of the data bits, up to 6. All bits -- 7 plus 3 plus 6 -- are stored as a word in memory. When a data word is entered into the register, a single count pulse will add ONE to the data word, which is then returned to memory.

In Figure A-9, P1 through P6 are the prescalers, D1 through D7 are data bits, and C1 through C3 are code bits. The code bits are decoded to provide one of six control inputs to a multiplexer chip. This chip accepts the selected prescaler output and feeds it to the remaining bits of the counter. If the code is 000, the count pulse bypasses all prescalers. The decoding at the lower left of Figure A-9 activates the prescalers in sequence per the code. For example, assume the code is 101 (decimal 5). Prescalers P1 through P5 are activated and the output of P5 is selected by the multiplexer.

A.5.3 Data Readout

Data readout is accomplished by a 10-bit shift register clocked at the desired rate for spacecraft acceptance. During readout, a memory word is fed to the data register and then to the shift register. The data register is reset to all zeros and the word returned to memory. After all words have been read out, the memory has been cleared by this process, ready for accumulation during the next period.

The shift register clocking for data readout is asynchronous to the system, so analysis and processing can go on while data is read out of the shift register.

A.5.4 Priority Scanner

Although the memory is organized in two halves, only a read or write operation is permitted from the entire memory at one time. Moreover, during accumulation of data, each half-memory is further divided. Words 1 through 130 are assigned to certain functions plus 125 channels of PHA-1, while word 131 is a function and the remaining 125 words take care of PHA-2.

64

(DATA ENTRY TO REGISTER NOT SHOWN)

Figure A-9.   Prescaling 16-Bit Data Register

A priority scanner is shown in Figure A-10.
Requests for service from PHA-1, PHA-2, and Data Readout
are scanned sequentially at a high rate by an 0-2 counter.
When a request is encountered, it sets a flip-flop to
stop the counter and permit the request to be serviced.
After the memory operation is completed, a clear signal
resets the flip-flop to restart the scanning.

A.5.5 Selectors

The data and address selectors are straight-
forward. Each bit is multiplexed by a single IC chip to
provide one address or data line as an output. Data
requires 16 chips while addresses require 8. See Fig-
ure 11.

A.5.6 Counters

Several counters are involved in the system. The
16-bit data register has already been discussed; in
addition to being a register, it is also a counter.

Each PHA includes a 7-bit counter chip. Output
from a PHA consists of a string of 1-MHz clock pulses and
these are counted to provide a digital representation of
energy. The resulting 7-bit word is an address in memory,
the 8th address bit being supplied separately to address
the appropriate channel. Each counter is reset by a
clear signal after that channel has been serviced.

A 9-bit counter supplies addresses for data readout.
Seven bits successively read out 128 words, bit 8 selects
the channel, and bit 9 controls the memory half-select
lines to select memory A or B. The counter consists of
a 7-bit counter chip and a dual J-K flip-flop.

Two time counters are clocked by a low-frequency
signal from the spacecraft, perhaps 30 to 60 Hz. The
counters are zeroed and started when memories A and B are
interchanged. Each word entered into the data register
is examined by an all-ones gate. Whenever a full-scale
word is detected, that address in memory is full so the
time counter and further analysis in that channel are
stopped. The time counter sends a signal to the mis-
cellaneous counter and the time word is entered at its
proper address in memory. Each counter is a 14-bit chip
and a dual flip-flop.
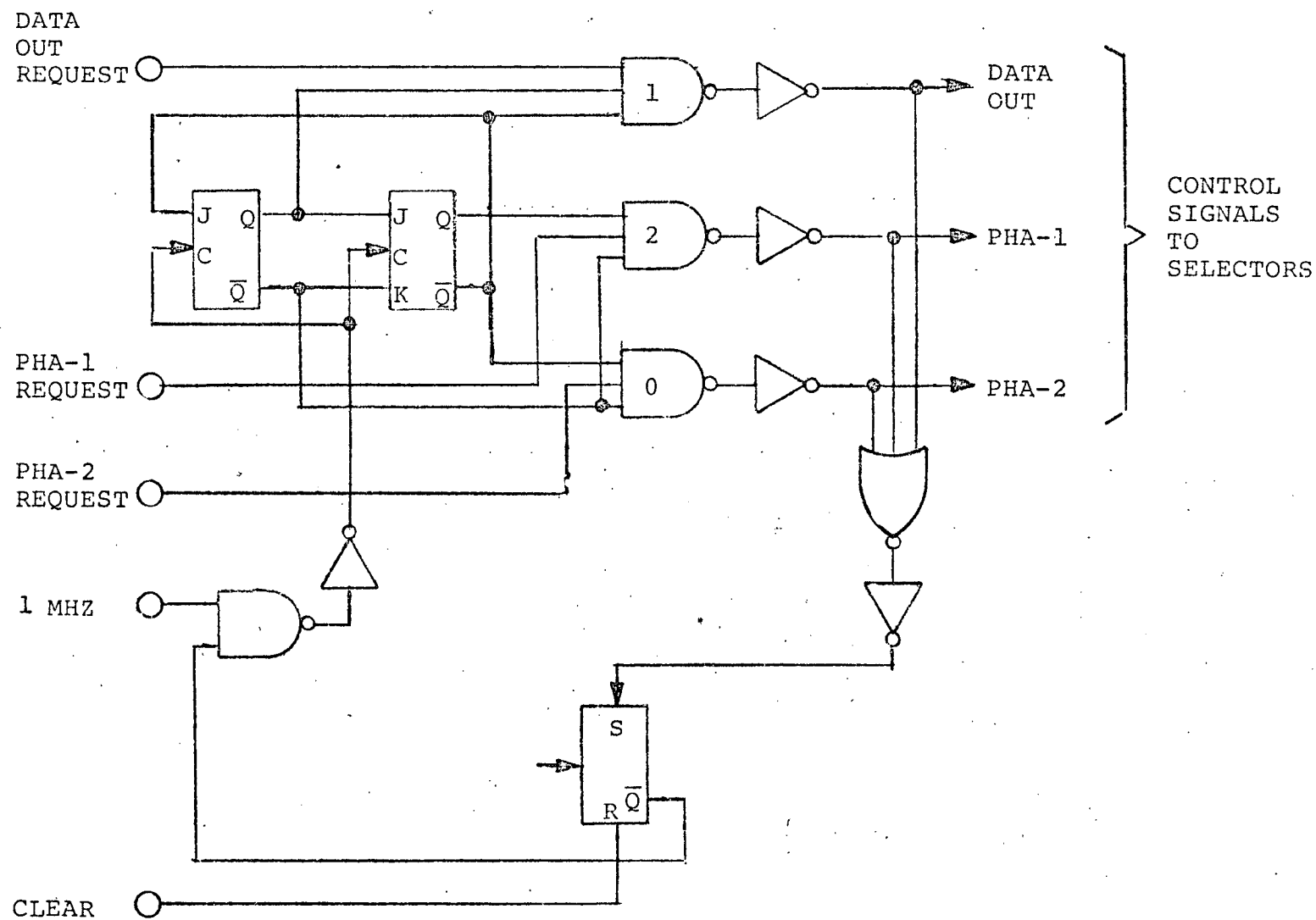
Figure A-10.   Priority Scanner

99

Figure A-11.   Data and Address Selector

The miscellaneous counter runs at memory clock rate and its purpose is to control memory entries of non-data words such as sync and time. The counter is a chip containing an 8-counter and decoder. Only those addresses up to 5 are of interest, since these are non-data words. If bit 8 is also high, the 3 address enters time word 2 as word 131.

A.5.7 Data readout

Data readout to the spacecraft is accomplished by a 10 bit shift register and a readout control circuit. A word is readout from memory into the data register and the last 10 bits -- seven data and three code bits -- are dumped into the shift register. Readout is under control of the shift clock at a rate determined by the spacecraft, while the analyzer goes on about its business. A frame sync input determines the accumulation period.

A.5.8 Timing and Control

A single box in Figure A-7 contains miscellaneous timing and control functions not discussed elsewhere.

68

APPENDIX B

MECHANICAL DESIGN AND PACKAGING

Based on the preliminary design of the X-RAY FLUORES-CENCE ANALYZER, a preliminary study of the mechanical design was completed. A parts list for the electronics (Appendix F) was derived from the circuit schematics and block diagrams. The types and quantities of the parts, together with the functional requirements of the circuits, led to the electronics packaging techniques presented below. The detector packaging is largely dictated by the requirements of the proportional counter itself, the window design approach, and the environmental constraints.

B.1 ELECTRONICS PACKAGING

The electronics for the X-RAY FLUORESCENCE ANALYZER will be contained in a magnesium enclosure approximately 3 inches by 7 inches by 8 inches* (168 cubic inches or 2.75 x 10^{-3}m^3) using contemporary techniques for packaging and fabrication. These techniques will be chosen to assure design and construction that will facilitate assembly, test, final checkout, and calibration of the system.

Analog circuits using discrete components will be designed as printed wiring cordwood modules (see Figures B-1 and B-2) mounted on two-sided printed wiring mother boards. This approach yields a favorable packaging density, while providing ease of fabrication and reworkability, both during fabrication and on-site repair in the field.

The logic circuits using flat-pack integrated circuits and the memory circuits using dual-in-line packages (DIP's) will be designed for installation on multilayer printed wiring boards. The multilayer printed wiring boards afford the most efficient and reliable method of packaging the complex interconnect of logic and memory circuitry while maintaining ease of fabrication, design flexibility and

---

*0.076 x 0.178 x 0.2m
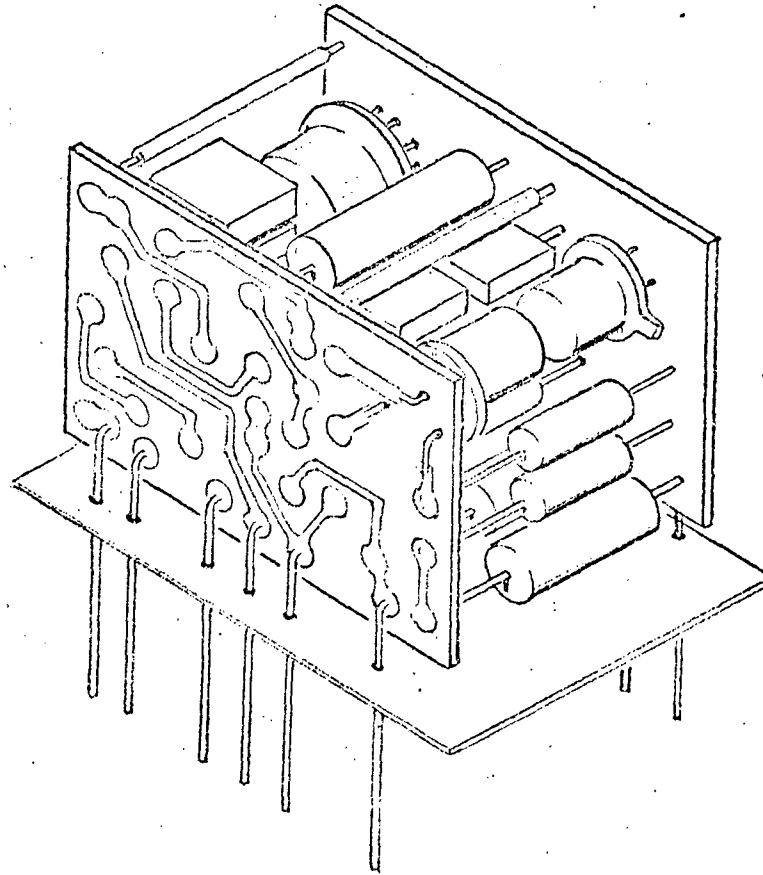
Figure B-1. Printed Wiring Cordwood Module

PRINTED WIRING
CORDWOOD MODULE

MAXIMUM
GROUND PLANE

CIRCUIT TRACE

OFF-PAD TERMINATION

MODULE LEAD
CLEARANCE HOLE

BIFURCATED
TERMINAL
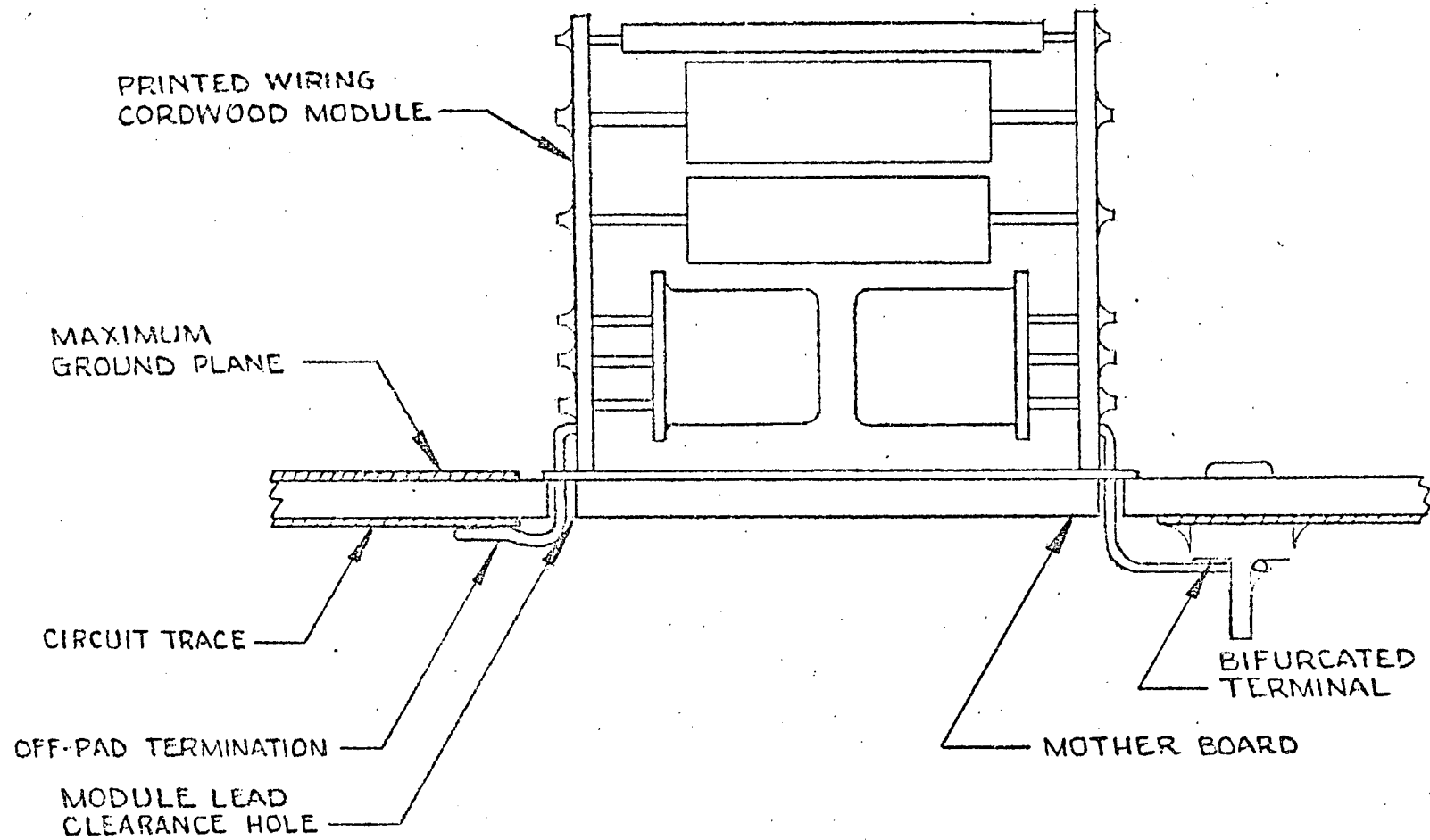
MOTHER BOARD

Figure B-2.   Cordwood Module/Mother Board

cost effectiveness. Figure B-3 shows the cover layer chip pattern for the flat-pack circuits that yields a packaging density of 5 flat-packs per square inch.

The design criteria for single and double-sided printed wiring boards are based on MSFC-STD-154 while multilayer printed wiring design criteria are based on MIL-P-55110.

In the high voltage power supplies, the packaging considerations are different from those related to the analog or low voltage circuits. Particular attention will be given to the prevention of breakdown or corona. Controlled spacings to limit voltage gradients, ball soldering to eliminate sharp points as a source of field emission, and potting of high voltage sections will be among the techniques used.

Figure B-4 shows an overall concept of the packaging of the analyzer electronics.

B.2 DETECTOR PACKAGING

The outboard-mounted detectors will be packaged to withstand the extreme temperature and atmospheric pressure to be encountered. A thin membrane honeycomb platform with thin-wall spacers will mechanically support and thermally isolate (in part) the detectors from the spacecraft outer shell. Consideration will be made as to the thermal control finish of the outside of the detector housings (not determined at the time of this writing). High temperature, high pressure seals will be employed in fabrication of the proportional counters. High voltage considerations will be made in the termination of the detector leads. A single, shielded, braided fiberglass-insulated wire, inside a thin-wall tube is one possible configuration being proposed.

The spherical sample window will be machined from a piece of beryllium stock to a wall thickness in the order of 0.015 inch (4.0×10^{-4} m) then chemically etched to the desired thickness (0.002 to 0.010 inch; 0.05 to 0.25 x 10^{-3} m). The spherical window will then be vacuum brazed to a 0.020 inch (5.08×10^{-4} m) thick stainless steel frame (using Al-SS Roll Bonded material). This frame and window will in turn be vacuum brazed to the main-frame using the same process. This process was selected over electron beam welding diffusion bonding or laser welding
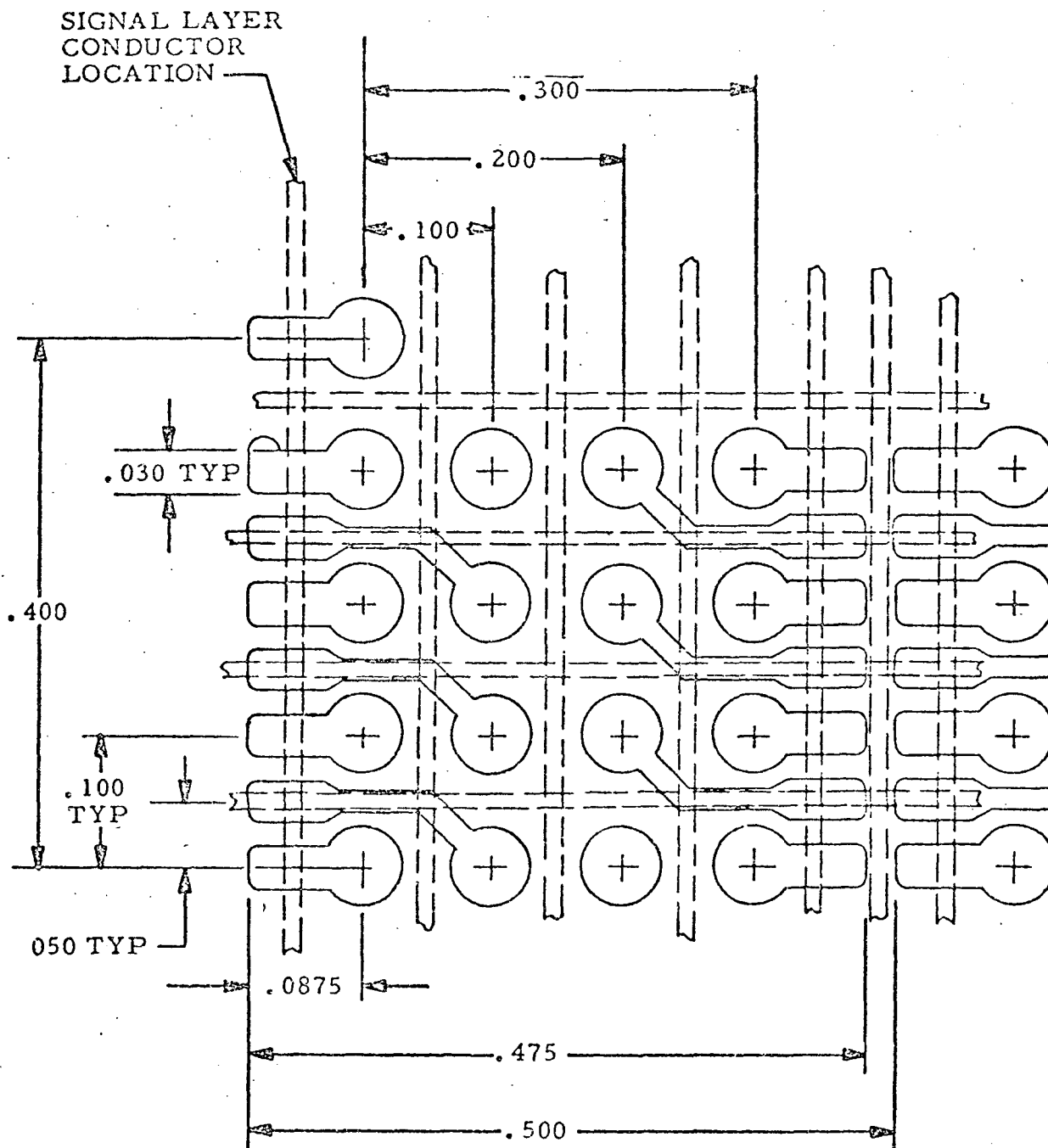
Figure B-3.   Cover Layer Chip Pattern

73

L.V. POWER SUPPLY

H.V. POWER SUPPLIES

INTRAWIRING CONNECTORS

UPPER HOUSING

SIGNAL PROCESSOR

H.V. LEADS TO DETECTORS

S/C INTERFACE CONNECTOR

MEMORY AND LOGIC

LOWER HOUSING

74
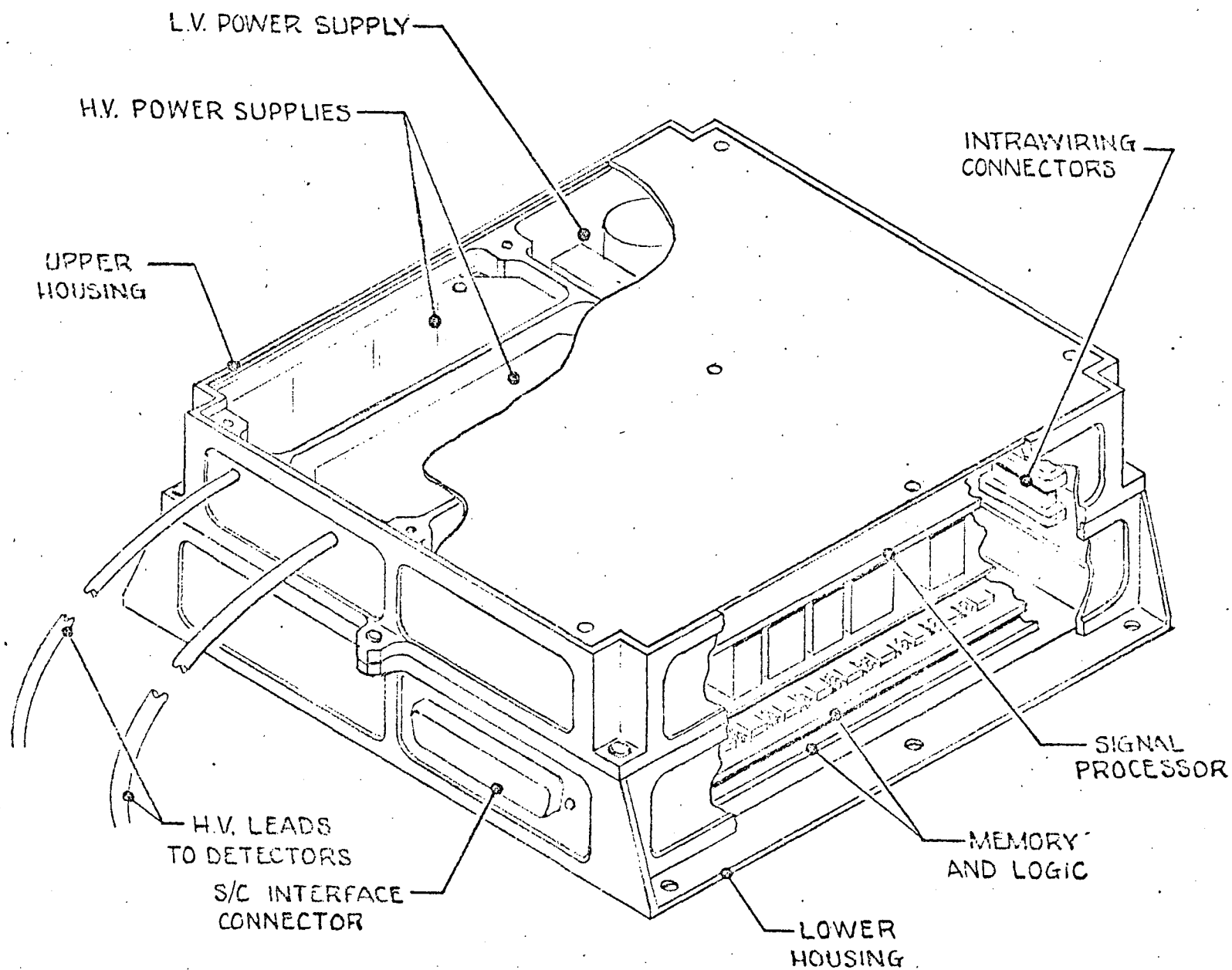
Figure B-4.   X-Ray Fluorescence Analyzer Electronics
(Conceptual Drawing)

as these welding methods tend to embrittle the material at the weld joint which would result in questionable weld integrity under the thermal and pressure environments to be encountered.

The detector window (between the soft x-ray primary source and the proportional counter) would be fabricated from commercially available rolled beryllium sheet. This detector window will then be vacuum brazed to a 0.020 inch (5.08 x 10^{-4} m) thick stainless steel frame (as with the sample window above). The frame and window will then be sealed to the adjoining chamber by gold wire "O"-ring.

The above recommended methods of fabricating the beryllium windows are not intended to imply final design decisions. It is planned that during the long-lead development stage, other candidate approaches such as grind forming, plating, explosive forming, and the like will be investigated. Because of the health hazards associated in the fabrication and handling of beryllium, only businesses experienced in the field have been consulted in connection with window fabrication.

Figure 1 (Section 1.0) shows a conceptual view of the two detectors.

B.3 WEIGHT ESTIMATE

Table III shows a weight estimate of the detectors and electronics of 2220 grams (4.9 pounds or 2.22 kg). (See Section 4.2.)

APPENDIX C

PROJECT SCHEDULE

76

UNIVERSAL MONITOR CORP.

SCHEDULE OF EVENTS	EXPERIMENT DEFINITION											EXPERIMENT IMPLEMENTATION																
TASK PHASE MO/YR	3 73	4 73	5 73	6 73	7 73	8 73	9 73	10 73	11 73	12 73	1 74	2 74	3 74	4 74	5 74	6 74	7 74	8 74	9 74	10 74	11 74	12 74	1 75	2 75	3 75	4 75	5 75	6 75
I LONG LEADTIME INSTRUMENT DEVELOPMENT	▨	▨	▨	▨	▨																							
1. Preliminary Design	▬	▬																										
2. Detector Design		▬	▬																									
3. Detector Fab. & Test				▬	▬																							
4. Interface and Support Definition						▬	▬																					
5. Test Equipment Preliminary Design						▬	▬																					
6. Order EM & GSE Parts						▬																						
7. Monthly Reports		▪	▪	▪	▪	▪	▪																					
II FABRICATE ENGR. MODEL												▨	▨	▨	▨	▨	▨	▨	▨									
1. Detail Design (Electronics)												▬	▬															
2. Breadboard													▬	▬														
3. Detail Design (Mechanical)														▬	▬													
4. Final Design Review															▪													
5. Release prototype and GSE drawings																	▬											
6. Build and test EM														▬	▬	▬	▬	▬										
7. Build and test GSE 1														▬	▬													
8. Order prototype and flight parts																	▬	▬										

X-RAY SPECTROMETER PROJECT SCHEDULE

UNIVERSAL MONITOR CORP.

SCHEDULE OF EVENTS	EXPERIMENT DEFINITION										EXPERIMENT IMPLEMENTATION																
TASK PHASE MO/YR	3 73	4 73	5 73	6 73	7 73	8 73	9 73	10 73	11 73	12 73	1 74	2 74	3 74	4 74	5 74	6 74	7 74	8 74	9 74	10 74	11 74	12 74	1 75	2 75	3 75	4 75	5 75	6 75
II (Cont'd)												▨	▨	▨	▨	▨	▨	▨										
9. Update design spec.															▭													
10. Monthly reports												▭	▭	▭	▭	▭	▭	▭	▭									
III FABRICATE PROTOTYPE																			▬	▬	▬	▬						
1. Build prototype																			▬	▬								
2. Test and evaluate																					▬	▬						
3. Final design review																							▭					
4. Release flight dwgs.																							▭					
5. Deliver proto. to ARC																							△					
6. Final ATP																					▭							
7. Build & test GSE 2																			▬	▬								
8. Order new parts																						▬						
9. Data package*																							▭					
10. GSE Manual																					▭							
11. Monthly reports																			▭	▭	▭	▭	▭	▭				

*As-built list, top assembly drawings & schematics, PL's, and test data.

X-RAY SPECTROMETER PROJECT SCHEDULE

78

UNIVERSAL MONITOR CORP.

SCHEDULE OF EVENTS		EXPERIMENT DEFINITION											EXPERIMENT IMPLEMENTATION																
TASK	PHASE MO/YR	3 73	4 73	5 73	6 73	7 73	8 73	9 73	10 73	11 73	12 73	1 74	2 74	3 74	4 74	5 74	6 74	7 74	8 74	9 74	10 74	11 74	12 74	1 75	2 75	3 75	4 75	5 75	6 75
IV	FABRICATE FLIGHT & REFURBISH PROTOTYPE																								▨	▨	▨	▨	
1.	Build flight model																								▬	▬			
2.	Test																										▬		
3.	Deliver to ARC																												△
4.	Data package																											▬	
5.	Refurbish prototype and deliver																									▬	▬		△
6.	Monthly reports																								▬	▬	▬	▬	
7.	Final report																									▬	▬		
8.	Field Support (2 men)																											▬	

X-RAY SPECTROMETER PROJECT SCHEDULE

APPENDIX D

DATA HANDLING

D.1 INTRODUCTION

The following discussion describes a preliminary definition of the techniques to be used for processing science data within the X-RAY FLUORESCENCE ANALYZER. The goal of the analysis is to define a system which provides the necessary data at minimum bit rate using reliable and proven hardware techniques.

D.2 DETECTOR CHARACTERISTICS

Each of the two detectors is a gas proportional counter which provides charge pulse outputs whose amplitudes contain the energy data of interest. The true energy spectrum is the superposition of a number of lines (monoenergetic sources) at the energies characteristic of the dust being analyzed. Amplitudes of the lines are determined in a complex way by the composition and thickness of the sample.

It is convenient to treat a single monoenergetic source at energy E_O. If the total mean count rate is R counts/sec, the distribution of charge content (pulse height) is approximately gaussian, and the observed count rate per unit energy at the detector output is

$$r(E) = \frac{2.35R}{\sqrt{2\pi}\ \Delta E_{PC}}\ \exp\left[-\frac{\left(E-E_o\right)^2}{2\left(\frac{\Delta E_{PC}}{2.35}\right)^2}\right]\ \frac{counts}{keV\text{-}sec} \qquad (1)$$

where ΔE_{PC} is the resolution of the counter expressed as full width of half maximum (FWHM). The corresponding rms deviation is $\sigma = \Delta E_{PC}/2.35$. Now in a proportional counter the chief cause of finite resolution in this energy range is simply statistical fluctuations in the number of primary electron-ion pairs formed. The counter resolution

is therefore expected to be proportional to $\sqrt{E}$, and this is found to be a good approximation. Typical resolution at the 5.9 keV Fe^{55} line is 18 percent FWHM. Thus

$$\Delta E_{PC} = 0.438 \; \sqrt{E} \; \text{(FWHM)} \tag{2}$$

From (1) and (2), the peak count rate is

$$r(E_o) = 0.938 \; \frac{R}{\Delta E_{PC}} = 2.14 \; \frac{R}{\sqrt{E}} \; \frac{\text{counts}}{\text{keV-sec}} \tag{3}$$

D.3 PULSE HEIGHT ANALYZERS

It is conventional to process spectral data by means of a pulse height analyzer (PHA) which sorts the detector pulses according to their apparent energies into bins of equal width. To conserve telemetry space, it is better to adjust the bin width to be some fixed fraction of the detector resolution which sets a fundamental limit on the information content of the spectrum. In this case, a quadratic PHA with resolution proportional to $\sqrt{E}$ is appropriate. Based on practical considerations in memory and logic organization, we have tentatively selected an offset quadratic characteristic as a compromise. For the high energy PHA, the channel number is

$$n \cong 58.5 \; \sqrt{E} \; -57.5 \tag{4}$$

so that n = 1 at 1 keV and 128 at 10 keV. The channel resolution at 1 keV is now 0.03 keV (14 channels FWHM). At 10 keV, ΔE_{PHA} is 0.12 keV (11.5 channels FWHM). Thus, the PHA resolution is still fairly well matched to the counter resolution.

For the low energy channel, the planned energy range is 0.5 to 5.0 keV, represented by

$$n \cong 81 \; \sqrt{E} \; -54 \tag{5}$$

The resulting PHA resolution ranges from 12 to 17 channels FWHM.

81

D.4 MEMORY

For each PHA, 125 memory channels will be required to accumulate a spectrum. Each memory channel will have a binary address, the last 7 bits of which are the PHA channel number. The data word stored at that address represents the accumulated count in the energy bin. In order that all channels of a given spectrum can be accumulated simultaneously over a relatively long period, two memory halves will be used simultaneously to accumulate one spectrum while the previous spectrum is read out.

To conserve telemetry space, it is desirable to use as short a data word as possible to represent the accumulated count in each energy channel. Any error resulting from data compression should be small compared to the statistical error of $\sqrt{N}$ counts rms in the mean count N. One scheme for accomplishing this end is described below.

Each memory channel has a 16-bit data word in which is stored the state of a 10-bit compressing accumulator with six prescaling flip-flops. The 10-bit data word is divided into a 7-bit binary counter and a 3-bit "range" counter which counts the number of times the 7-bit counter overflows and inserts prescaling flip-flops, as follows.

7-Bit Counter Contents	Range	Number of Prescaling Flip-Flops	Actual Count	Maximum Compression Error
00000	000	0	0	0
11111	000	0	127	0
00000	001	1	128	±1
11111	001	1	382	±1
00000	010	2	384	±2
11111	010	2	892	±2
00000	011	3	896	±4
–	–	–	–	
–	–	–	–	
–	–	–	–	
–	–	–	–	
11111	101	5	8,032	±16

7-Bit Counter Contents	Range	Number of Prescaling Flip-Flops	Actual Count	Maximum Compression Error
00000	110	6	8,064	±32
11111	110	6	16,192	±32
00000	111	6	16,256	±32
11111	111	6	24,384	±32

The maximum fractional compression error in the counter is 1/128 or 0.8 percent. Figure D-1 shows the compression error as a function of count, together with the statistical error.

D.5 DATA READOUT AND COUNT RATE

Assuming a data accumulation and readout period of 10 minutes, the readout bit rate required is computed as follows. We must read out 125 channels for each detector. Allow three additional 10-bit data words for timing, synchronization and housekeeping. Then the number of bits to be read out is

$$128 \times 10 = 1280 \text{ bits per spectrum} \tag{6}$$

For two detectors, the total bit rate is

$$\frac{2 \times 1280}{600} = 4.27 \text{ bits/sec} \tag{7}$$

From equation (3), the count rate in the peak channel for the high energy detector is about

$$r(E_o) \left. \Delta E_{PHA} \right|_{E-E_o} = \left(2.14 \frac{R}{\sqrt{E}} \right) \times (0.03 \sqrt{E})$$

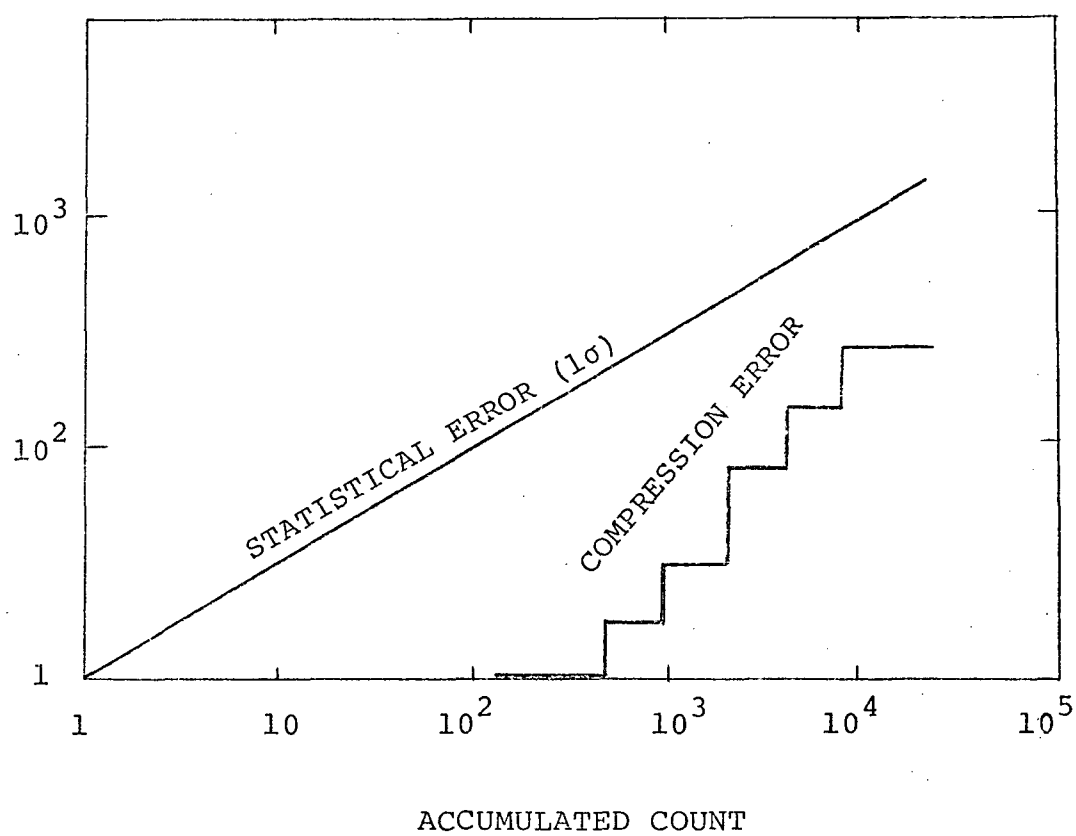$$= 0.06R \frac{\text{counts}}{\text{sec}} \tag{8}$$

83

Figure D-1. Data Compression and Statistical Errors

84

If the count rate for a single peak satisfies

$$R \leq \frac{24,384}{600 \times 0.06R} = 675 \text{ counts/sec} \tag{9}$$

then the memory will not overflow in the accumulation period. It is necessary to accommodate a wide range of count rates because the thickness of the dust layer is so uncertain. The obvious method is to design the instrument to give as high a count rate as the detector will tolerate, then adjust the accumulation time to avoid memory overflow. This can easily be accomplished by simply examining the PHA counter value before incrementing, and stopping accumulation when any channel reaches full capacity. The spectrum would then have the appearance shown in Figure D-2.

By recording and transmitting the time at which accumulation was stopped, the actual count rate will be known. The maximum accumulation time would be held at 10 minutes to assure a minimum number of spectra; successive spectra could be averaged on the ground (within the limits of the compression error) to improve statistical precision.
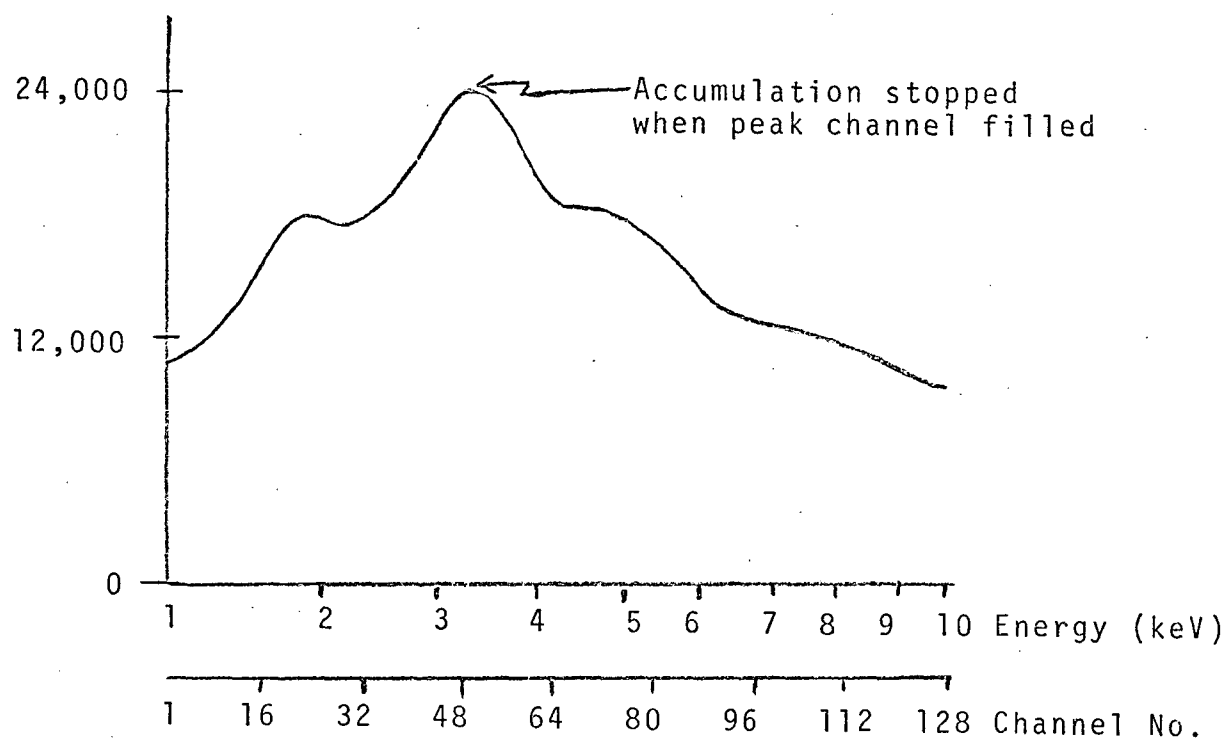
Figure D-2. Typical Spectrum

86

APPENDIX E

COST ESTIMATE

VENUSIAN FLUORESCENCE ANALYZER

PHASE I	LONG LEADTIME INSTRUMENT DEVELOPMENT	$ 81,010	
	Escalation Cost*	7,290	$ 88,300
PHASE II	FABRICATE ENGINEERING MODEL	193,245	
	Escalation Cost*	17,392	210,637
PHASE III	FABRICATE PROTOTYPE	155,699	
	Escalation Cost*	14,013	169,712
PHASE IV	FABRICATE FLIGHT AND REFURBISH PROTOTYPE	135,185	
	Escalation Cost*	12,167	147,352
	TOTAL		$616,001**

---

*Includes 9% escalation cost of labor, materials, and ODC.

**If lower count rates are acceptable, less expensive radiation sources can be used and the total price can be reduced significantly.

87

COST BREAKDOWN

PHASE IV - FABRICATE FLIGHT & REFURBISH PROTOTYPE

LABOR

Category	Hours	Rate	Total
Physicist	100	$10.00	$ 1,000
Project Engineer	300	14.00	4,200
Mechanical Engineer	100	9.00	900
Electronic Engineer	150	8.00	1,200
Sr. Electronic Technician	740	6.00	4,440
Draftsman	60	4.50	270
Assembler	1740	4.50	7,830

$ 19,840

Overhead (112%)   22,221

$ 42,061

MATERIAL   20,000

SUBCONTRACTS (including refurbishment)   40,000

TRAVEL: Ames (2 men x 5 days x 2 trips)*   636

East Coast (2 men x 2 days x 2 trips)**   1,760

CONSULTANT   -0-

ODC (Environmental testing, misc.)   500

$104,957

G&A (15%)   15,744

$120,701

FEE (12%)   14,484

TOTAL PRICE $135,185

---

*[$34 x 2 x 2] + [$50 x 5 x 2] = 136 + 500 = $636

**[$340 x 2 x 2] + [$50 x 2 x 2 x 2] = 1360 + 400 = $1,760

COST BREAKDOWN

PHASE II - FABRICATE ENGINEERING MODEL

LABOR

Category	Hours	Rate	Total
Physicist	500	$10.00	$ 5,000
Project Manager	560	14.00	7,840
Mechanical Engineer	580	9.00	5,220
Electronic Engineer	1120	8.00	8,960
Sr. Electronic Technician	1120	6.00	6,720
Draftsman	1000	4.50	4,500
Assembler	500	4.50	2,250

	$40,490
Overhead (112%)	45,349
	$85,839
MATERIAL (Instrument & GSE)	22,000
SUBCONTRACTS (Housings, PC Boards, Radiation Sources, etc.)	38,000
TRAVEL: Ames (2 men x 1 day x 4 trips)*	336
East Coast (2 men x 2 days x 2 trips)**	1,760
CONSULTANT: ME ($20 x 80)	1,600
ODC	1,000
	$150,035
G&A (15%)	22,505
	$172,540
Fee (12%)	20,705
TOTAL PRICE	$193,245

---

*[$34 x 2 x 4] + [$50 x 4] = $336

**[$340 x 2 x 2] + [$50 x 2 x 2 x 2] = 1360 x 400 = $1,760

COST BREAKDOWN

PHASE I - LONG LEADTIME INSTRUMENT DEVELOPMENT

LABOR

Category	Hours	Rate	Total
Physicist	580	$10.00	$ 5,800
Project Manager	140	14.00	1,960
Mechanical Engineer	600	9.00	5,400
Electronic Engineer	350	8.00	2,800
Sr. Electronic Technician	200	6.00	1,200
Draftsman	100	4.50	450
Assembler	50	4.50	225

			$17,835

Overhead (112%)   19,975

      $37,800

MATERIAL   4,000

SUBCONTRACTS (Machining, etc.)   17,000

TRAVEL - Ames (2 men x 1 day x 2 trips)*   236

        East Coast (2 men x 2 days x 2 trips)**   1,760

CONSULTANT (Mech. Engr. $20/hr x 80 hrs)   1,600

ODC   500

      $62,896

        G&A (15%)   9,434

      $72,330

        Fee (12%)   8,680

           TOTAL PRICE $81,010

---

*[$34 (airfare) x 2 x 2] + [$50 x 2] = $236

**[$340 (air) x 2 x 2] + [$50 (car plus expenses) x 2 x 2 x 2]
= $1,760

APPENDIX F
PARTS LIST

Neither component types nor quantities should be considered as final, since the list was intended primarily for use in determining package size, configuration, and weight, and in arriving at a reasonalbe parts cost figure.

Quantity	Item	Description
6	2N4867A	FET
4	2N3799A	Low-Noise PNP
8	2N3117	Low-Noise NPN
8	2N4044	Dual NPN
7	2N4045	Dual NPN
6	2N3811	Dual PNP
48	2N2222A	NPN
20	2N2907A	PNP
2	2N2369A	High-Frequency NPN
4	2N3723	Power Switch NPN
2	2N5906	Dual FET
1	1N827	Zener
62	1N4148	Diode
10	1N3070	Rectifier
60	RNR55	1% Film Resistor
240	RCR05	5% Carbon Resistor
31	CKR05	Ceramic Capacitor
57	CKR06	Ceramic Capacitor
36	CSR13	Tantalum Capacitor
23	Erie Disc	High Voltage
9	90537	Nytronics Inductor
10		Feed-through Capacitor
3		Power Transformer (Toroidal)
1		Thermistor
1		Delay Line
12		High-Voltage Resistor
24		High Voltage Rectifier

C2

Quantity	Item	Description
11	SG-0001A	National Semiconductor Amplifier
2	Reynolds Industries	High Voltage Coaxial Connector
2	Dale	Low Voltage Coaxial Connector
1	Cannon	25-pin Connector
1	Cannon	37-pin Connector
6	Cannon	Misc. Connector

Total Quantity
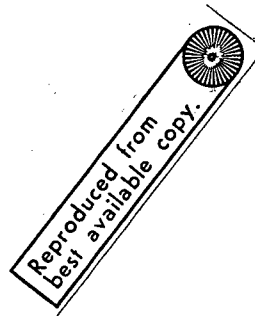
710 components
  8 connectors
 32 IC memory chips
 8υ IC logic chips
_____
830

92

Computer Program

```
 1 R1=0.127
>2 B=0.127
>3 L=R1+B+0.318
>4 Z1=0.785
>5 R2=R1+L*TAN(Z1)
>6 X1=-R2
>7 X2=R2
>29 P0=ATN(R1/(B+R1))
>30 P1=P0/10
>35 P=P1/2
>39 N=1
>40 H=N*.1E-4
>50 W1=0.834
>55 W2=0.342
>60 M1=129.7
>65 T1=1.77E-2
>70 M2=0.18
>75 T2=5.6E-3
>80 M3=12
>85 T3=2.8E-3
>90 M4=150
>95 M5=4.3
>100 M6=8.65
>105 V=0
>106
>109
>290 IF P>P0 THEN 300
>SAVE OVER FOSTER
>
```

```
 LIST
 1 R1=0.127
 2 B=0.127
 3 L=R1+B+0.318
 4 Z1=0.785
 5 R2=R1+L*TAN(Z1)
 6 X1=-R2
 7 X2=R2
 10 DEF FNU(X)=-SQR(R2^2-X^2)
 15 DEF FNW(X)=SQR(R2^2-X^2)
 20 K=3.7E10
 25 K1=0.03979
 29 P0=ATN(R1/(B+R1))
 30 P1=P0/10
 35 P=P1/2
 39 N=1
 40 H=N*1E-4
 45 S=0.1
 50 W1=0.834
 55 W2=0.342
```

93

Computer Program (Continued)

```
55  W2=0.342
60  M1=129.7
65  T1=1.77E-2
70  M2=0.18
75  T2=5.6E-3
80  M3=12
85  T3=2.8E-3
90  M4=150
95  M5=4.3
100 M6=8.65
105 V=0
110 D1=2*X2/30
115 D2=H/30
120 D3=2*X2/30
125 Q1=(B+R1)*SIN(P)/R1
130 Q2=SQR(1-Q1^2)
135 S1=1/Q2
140 C= Q2*COS(P)+Q1*SIN(P)
145 A=B+0.3+R1*(1-C)
150 E1=A/C
155 D=(B+R1*(1-C))*TAN(P)
160 K2= K*K1*(S*W1/(M1*T1))*SIN(P)*P1*M6*W2*A*S1
165 K3=(1-EXP(-M1*T1))*EXP(-M2*T2*S1)
175 X=X1
180 Y=0
185 Z=FNU(X)
190 G=SQR(A^2+X^2+(D+Z)^2)
195 S2=(2*E1*G/A^2)/(1+1/C^2)
200 S3=G/A
205 Q3=EXP(-M3*Y*S1)*EXP(-M4*Y*S2)
210 Q4=EXP(-M5*T2*S2)*EXP(-M5*T3*S3)
215 Q5=1/G^3
220 F=K2*K3*Q3*Q4*Q5
225 V=V+F*D1*D2*D3
230 Z=Z+D3
235 IF Z>FNW(X) THEN 245
240 GO TO 190
245 Y=Y+D2
250 IF Y>H THEN 260
255 GO TO 185
260 X=X+D1
265 IF X>X2 THEN 275
270 GO TO 180
275 PRINT
280 PRINT "INTEGRAL="V
285 P=P+P1
290 IF P>PO THEN 300
295 GO TO 125
300 END
>
```

Revised 3/20/73

94
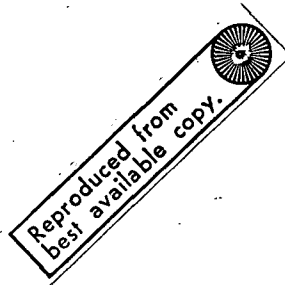
APPENDIX (G)

VOCABULARY

Original Notation	Computer Notation
r_2	R1
y	B
ℓ	$\dot{L}$
$\mathfrak{I}$	Z1
r_3	R2 $(= r_2 + \ell \tan \mathfrak{I})$
$-(r_2 + \ell \tan \mathfrak{I})$	X1
$+(r_2 + \ell \tan \mathfrak{I})$	X2
3.7×10^{10}	K
$\dfrac{1}{8\pi}$	K1
$\alpha_\circ$	P0
$\Delta\alpha$	P1
α	P
n	N
$n \times 10^{-4}$	H
S	S
W_1	W1
W_2	W2
t_1	T1
t_2	T2
t_3	T3
μ_1	M1
μ_2	M2
μ_3	M3
μ_{ij}	M4
μ_{ik}	M5
μ_{ip}	M6

- - - - - - - - - - - - -

x	X
y	Y
z	Z

95   Revised 3/20/73

Test Problem Printout and Data Sheet

```
>55 W2=0.043
>100 M6=1.44
>90 M4=3835
>95 M5=178
>RUN
14:40    12/15

INTEGRAL= .568080

INTEGRAL= 2.28568

INTEGRAL= 5.19435

INTEGRAL= 9.36931

INTEGRAL= 14.9308

INTEGRAL= 22.0656

INTEGRAL= 31.0698

INTEGRAL= 42.4413

INTEGRAL= 57.1171

INTEGRAL= 77.2654


300 HALT
>
```

```
>
!BYE
12/15/   '72 14:54
CPU TIME 52.553
I/O WAIT TIME 0.008
MON SERVICES 0.021
```
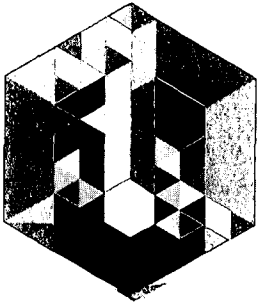
Revised 3/20/73

DATA SHEET

Source _C d^{109}_ $\quad$ W_1 _0.834_ $\quad$ t_1 _1.77 × 10^{-2} cm_

Sample _Olivine dust_ $\quad$ Element analyzed _Si_

W_2 _0.043_ $\quad$ n _100_ $\quad$ t_2 _0.0056 cm_ t_3 _0.0028 cm_

$\mu 1$ _129.7 cm^{-1}_ $\quad$ $\mu 2$ _0.18 cm^{-1}_ $\quad$ $\mu 3$ _12 cm^{-1}_

μip _1.44 cm^{-1}_ $\quad$ μij _3835 cm^{-1}_ $\quad$ μik _178 cm^{-1}_

r_2 _0.127 cm_ ξ _0.755 rad_ $\quad$ y _0.127 cm_ $\quad$ ℓ _0.572 cm_

K = 0.850 $\qquad$ (N_i) $\qquad$ (N_{ic})

Count rate $\quad$ — 77.3 $\qquad$ 65.7

ξ		y		Count rate	
ξ		y		Count rate	
ξ		y		Count rate	
ξ		y		Count rate	
ξ		y		Count rate	
ξ		y		Count rate	
ξ		y		Count rate	
ξ		y		Count rate	
ξ		y		Count rate	
ξ		y		Count rate	
ξ		y		Count rate	
ξ		y		Count rate	
ξ		y		Count rate	
ξ		y		Count rate	
ξ		y		Count rate	
ξ		y		Count rate	
ξ		y		Count rate	
ξ		y		Count rate	

Revised 3/20/73

March 20, 1973

Mr. Gabriel Fox
Contract Officer
NASA, Ames Research Center
Moffett Field, Ca. 94035

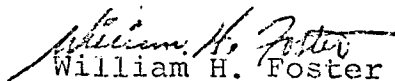Reference: Contract No. NAS2-7356

Dear Mr. Fox:

Enclosed, please find six copies of the FINAL REPORT
prepared on subject contract. These reports incorporate
comments and suggestions received from the NASA/ARC Technical
Officer. The reports constitute fulfillment of all contrac-
tual obligations.

In addition, you will find an enclosure which responds to
random questions received from various technical personnel, as
noted, at NASA/ARC. The questions seemed best answered in
this format because they did not fit conveniently into the
report.

I believe the information is all self explanatory. How-
ever, should questions arise, I shall be pleased to receive
them at your earliest convenience.

Cordially,

UNIVERSAL MONITOR CORPORATION

William H. Foster
General Manager

WHF:lf

Enclosures

cc: Mr. M. Blanchard,
     Technical Officer, ARC

Per D. Webster

Section 3.1.2:

(a) and (b) and one he missed have been picked up and incorporated.

(c) A subscripted letter was used to avoid an even more clumsy notation later on.

(d) Dave answered the first question himself and had similar shielding in his own window-source design. We are trying to minimize scattered primary radiation. It is serious because it contributes to the background count rate and could obscure counts from fluorescent x-rays because of counter dead time. It could also (through Compton scattering) give rise to false positives. We have not specified a material for the support cone except by inference (stainless steel). Iron (or steel) would not be a good choice if primary rays are allowed to reach the support cone regardless of the source. Scattering of x-rays depends upon the atomic number of the scatterer. Resonance absorption might be a good idea if x-rays were only scattered by the K-electrons, but this just isn't the case. If a design is chosen where the support is in the primary beam, it should be fabricated of beryllium, not of a high-Z material.

(e) The part of the upper window not in the primary beam could be considered to be a part of the window support and is necessary to avoid bending stresses. We are supporting the window in the only way possible which eliminates bending stresses.

(f) The symbol w_1 was defined on page 12, line 2.

(g) The fluorescence yield of the elements in question is listed in the Table on page 28 under the column heading "$W_2K\alpha$". We have rewritten portions of the text, replacing inferences with direct references.

(h) We hang our heads in shame. The typist skipped two lines in the rough draft. After typing A_{Dp} she dropped down to the definition of A_{Ds} and typed it for A_{Dp} and then, of course, omitted A_{Ds} completely. Unfortunately, this error was not caught in the first proofreading because of the haste with which it was prepared.

(i) Subscripts under a summation sign are always local. For the benefit of those unacquainted with this convention, we have changed our subscripts to eliminate possible confusion.

(j) We tried to cooperate by doing in four weeks a job which we estimated would require from six to eight weeks and, therefore, apologize for the confusion which resulted from our failure to catch a number of typist errors before the report was shipped.

Section 3.1.3

(a) Our purpose here was not to write a dissertation on x-ray fluorescence but to provide a bare-bones outline upon which the calculations of the volume of source material required could be based. Failure to discuss the quantum mechanical aspects of Auger transition probabilities does not mean that we are unaware of their importance. The definition of w_1 on page 12 and the inclusion of fluorescence yields in the table on page 28 showed that we were acquainted with the concept of fluorescence yield and had included it in our calculations.

(b) We did not have time to optimize source geometry. The calculations show that this geometry will give adequate count rates for very thin dust layers. The "inefficiency" objected to is a part of the trade-off necessary to approximate a point source and thus minimize scattered primary radiation and source shielding of the lower window.

RESPONSE TO COMMENTS

Per D. Cunningham

1. Section 3.1.1 Stress Analysis, p. 7.

We do not understand the question. Your formula is the same as that in our report.

2. Section 3.1.1 Stress Analysis, p. 11.

W. Rihn, one of the senior mechanical engineers consulted, states: "A machined beryllium hemisphere would include an integral flange somewhat thicker than the window portion of the sphere. This makes mounting of the hemispherical window relatively easy by brazing. A cylindrical window fabricated from beryllium foil presents difficulties in attachment as it would probably have to be electron-beam welded to the window frame and the frame brazed to its support structure. This adds considerably to the fabrication problem and supports the conclusion that fabrication of the hemispherical window is less difficult than for the cylinder." See also the attached copy of a report from T. Parker, another senior mechanical engineer who studied this problem.

3. Section 3.1.3 Window Design Calculations, p. 20.

One supplier (Isotope Products Laboratories) has offered to produce sources which are initially almost 100% pure Fe^{55}. While the volume calculations assume pure Cd^{109} in the case of the higher energy source, it might be wise to use cadmium chloride. The melting point of cadmium is about $321^{\circ}C$ whereas cadmium chloride melts at 568°. If the source is well isolated thermally and/or well contained, a pure Cd^{109} source would probably be satisfactory.

4. Section 3.1.3, p. 21.

This is a good point. We have recalculated the linear absorption coefficients in olivine dust and in silica dust, assuming 30% of the volume to be taken up with carbon dioxide gas at 100 atmospheres pressure. This produced an increase in the absorption coefficient of oxygen of about 5%, but the composite absorption coefficients increased less than 2%. Thus, the error introduced by neglecting the presence of CO_2 is smaller than many other uncertainties in these calculations. To substantiate this statement we reran one calculation using linear absorption coefficients which included the effects of CO_2. Neglecting the CO_2 the count rate was 51.95; when CO_2 was included, the count rate was 51.79 (uncorrected count rates, c_i).

5. Section 3.1.3, p. 24.

Sorry. The window thickness was 0.0056 cm throughout all calculations. This has been noted in the text of the report.

6. Section 3.1.3, p. 26.

See the revised Table on page 26 for the results of a run using an Fe^{55} source to analyze for silicon in olivine.

7. Section 3.1.3, p. 29.

The text has been revised to reflect the narrower range of elements called out. One calculation was run using the data for the large, thick window. The results are given in the report following the proposed window dimensions.

8. Section 3.1.3

A listing of the computer program, a test run, and a corresponding data sheet are placed in an appendix.

<u>FORMING AND JOINING OF A BERYLLIUM WINDOW</u>

Forming

The task is to fabricate a Beryllium window ¼" wide by 1" long and 0.002 to 0.005" thick with corrugations every 0.080" along its length.

The window will be subjected to 90 to 100 atmospheres differential pressure and an ambient temperature of 500°C.

Breathing of beryllium dust particles is a health hazard, and therefore any operation which may possibly create fine particles must be done under conditions which prevent any possible breathing of these particles. All machining poerations must be done under conditions where the particles created are collected at the tool and isolated in a container which precludes their discharge into the atmosphere. Heating operations such as welding and brazing must be similarly controlled. Only those companies which have the experience and special equipment should be considered for forming or joining the window.

The following methods were considered for forming the window.

Hot Forming

A beryllium sheet would be rolled to about 0.020" thick then chemically milled to 0.002" or 0.005". as desired. The sheet is not rolled to the thin thickness because beryllium is susceptible to developing directionality in properties because of working. Often good ductility is present in one direction while being very poor in other directions. One method used in sheet production

is to cross roll.   A designer should be aware of
these directional properties and siscuss hes
requirements with his supplier.

The forming of the corrugations would be done at
an elevated temperature in a furnace using a
corrugating roller that would form one corrugation
at a time.   The easiest form of these corrugations
to form would be a gentle sign wave.   This method.
has been used succesfully by George Cremmer of Solar.

Solar
Division of International Harvester
San Diego, California
714-233-8241

Solar has complete facilities for handling and
processing beryllium and may even have tooling
which could be used for this application. Solar
has made beryllium windows for Neutron and XRay
detectors for a number of space programs and at
present is makeing a window 40" xx 60" xx 0.002".
They have also made honey comb structures of
beryllium.

Chemical Milling

Chemical milling the corrugated shape might be
possible but George Cremmer of Solar said that
it would be extremely difficult.   If more
information is desired he suggested contacting
Lockheed Aircraft Co.

Grind Forming

It might be possible to form the corrugations
using shaped grinding wheels but it is not
recommended because of the danger of the powder
formed during grinding.

Plating

It might be possible to form the corrugated
shape by plating beryllium on to a shaped
cathode but I was unable to find any one interested.

Electrical Discharge Machining (EDM)

EDM presents many of the same problems as grinding also I could not find anyone interested in working with beryllium.

Explosive Forming

I was unable to find a source in this short time.

Joining

The following methodes were considered for joining the beryllium window to 300 series stainless steel.

Vacuum Brazing

Brazing of beryllium is practicable using either conventional aluminum brazing alloys or silver brazing alloys or an Aluminum-Stainless Steel Roll-Bonded material. High nickel alloys and monel have also been used successfully. Joints with leak rates of less than 1×10^{-9} cc/sec have been made with the Al-SS Roll Bonded material according to Wayne Marcellin of Electrofusion.

> Electrofusion
> 104 Constitution Dr.
> Menlo Park, California
> 415-324-0074

Electrofusion has fabricated beryllium windows for Neutron Detedtors for E.G.&G?. and Varian.

Wayne Marcellin recommends either the Al-SS Roll Bond material or pure silver as a filler material for brazing beryllium to S.S..

Solar of San Diego also has extensive experience with brazing beryllium to S.S. George Cremmer of Solar suggested brazing a 0.020" "picture" frame around the corrugated window then brazing that to the stainless steel.

Electron Beam Welding

Welding of beryllium results in brittle welds
which have not at present been considered
satiffactory. Hamilton Standard has welded
beryllium to steel but I was unable to get any
data on their success at his time.

Diffusion Bonding

Livermore Radiation Lab. has been doing work
on this process but I think it would require
considerable development for this particular
application.

Laser Welding

I was unable to find anyone to do this but it
would probable also result in brittle welds.

Mechanical Clamping

Mechanical clamping of the window with a gold
O-ring seal would have the advantage of being
resealable but would have the disadvantage of
excess weight and space for the sealing surface
and screws.

I was unable to find any local sources for forming or
joining of beryllium. Those that I contacted either
were not interested or refered me to Solar or Electrofusion.

106   Ted Parker